The LIF-Mediated Molecular Signature Regulating Murine Embryo Implantation 1

Authors: Rosario, Gracy X., Hondo, Eiichi, Jeong, Jae-Wook, Mutalif, Rafidah, Ye, Xiaoqian, et al.

Source: Biology of Reproduction, 91(3)

Published By: Society for the Study of Reproduction

URL: https://doi.org/10.1095/biolreprod.114.118513

BIOLOGY OF REPRODUCTION (2014) **91**(3):66, 1–18
Published online before print 16 July 2014.
DOI 10.1095/biolreprod.114.118513

The LIF-Mediated Molecular Signature Regulating Murine Embryo Implantation[1]

Gracy X. Rosario,[3] Eiichi Hondo,[4] Jae-Wook Jeong,[5] Rafidah Mutalif,[3] Xiaoqian Ye,[3] Li Xuan Yee,[3] and Colin L. Stewart[2,3]

[3]*Developmental and Regenerative Biology, Institute of Medical Biology, A*STAR, Immunos, Singapore*
[4]*Laboratory of Animal Morphology, Division of Biofunctional Development, Graduate School of Bioagricultural Sciences, Nagoya University, Nagoya, Japan*
[5]*Department of Obstetrics and Gynecology and Reproductive Biology, Michigan State University, Grand Rapids, Michigan*

ABSTRACT

The establishment of a receptive uterus is the prime requirement for embryo implantation. In mice, the E_2-induced cytokine leukemia inhibitory factor (LIF) is essential in switching the uterine luminal epithelium (LE) from a nonreceptive to a receptive state. Here we define the LIF-mediated switch using array analysis and informatics to identify LIF-induced changes in gene expression and annotated signaling pathways specific to the LE. We compare gene expression profiles at 0, 1, 3, and 6 h, following LIF treatment. During the first hour, the JAK-STAT signaling pathway is activated and the expression of 54 genes declines, primarily affecting LE cytoskeletal and chromatin organization as well as a transient reduction in the progesterone, TGFbetaR1, and ACVR1 receptors. Simultaneously 256 genes increase expression, of which 42 are transcription factors, including *Sox, Kfl, Hes, Hey*, and *Hox* families. Within 3 h, the expression of 3987 genes belonging to more than 25 biological process pathways was altered. We confirmed the mRNA and protein distribution of key genes from 10 pathways, including the Igf-1, Vegf, Toll-like receptors, actin cytoskeleton, ephrin, integrins, TGFbeta, Wnt, and Notch pathways. These data identify novel LIF-activated pathways in the LE and define the molecular basis between the refractory and receptive uterine phases. More broadly, these findings highlight the staggering capacity of a single cytokine to induce a dynamic and complex network of changes in a simple epithelium essential to mammalian reproduction and provide a basis for identifying new routes to regulating female reproduction.

implantation, LIF, luminal epithelium, microarray, uterus

INTRODUCTION

Attainment of a receptive state by the uterus is a prerequisite for successful embryo implantation and placental development. The transition of the uterus from a hostile, nonreceptive state for the embryo to a receptive environment is primarily driven by the actions of the two ovarian sex steroid hormones: progesterone (P4) and estrogen (E_2) [1–3]. In the mouse, despite the presence of adequate P4, the uterus remains refractory to blastocyst attachment until the morning of Day 4 of pregnancy (Day of Plug = D1) when the ovary secretes a second wave of E_2, termed nidatory E_2. This wave converts the nonreceptive uterine luminal epithelium (LE), consisting of a single layer of epithelial cells lining the lumen, to a state favoring blastocyst implantation. Conversion of the LE allows both invasion of the uterus by the embryonic trophoblast as well as inducing decidualization of the underlying stroma [4, 5].

In murine reproduction, the primary function of nidatory E_2, in conjunction with the tumor suppressor/transcription factor p53, is to induce synthesis of the cytokine leukemia inhibitory factor (LIF) [6–8], with LIF being expressed in the uterine endometrial glands (or glandular epithelium [GE]) just prior to the onset of implantation [9, 10]. In many other mammalian species, including humans, LIF levels increase at the onset of implantation, suggesting it is key to regulating implantation throughout the mammalian clade [11, 12]. Female mice lacking the LIF gene are infertile due to implantation failure. However, LIF-null embryos can implant normally when transferred to wild-type pseudopregnant females, revealing that a maternal defect is responsible for the implantation failure [6]. Furthermore, a single injection of LIF substitutes for nidatory E_2 at initiating blastocyst implantation, stromal decidualization, and successful postimplantation development in ovariectomized pregnant female mice maintained on P4 [6, 7].

LIF is secreted into the uterine lumen where it binds to LIF receptors (LIFRs) on the LE [13, 14]. LIF binds to the heterodimeric LIFR complexes, consisting of two transmembrane proteins LIFR and gp130. Activation of the LIF-LIFR-gp130 complex phosphorylates the signal transducer and activator of transcription factor 3 (STAT3) and MAP kinase pathways [15]. Phosphorylated STAT3 dimerizes and then accumulates in the nucleus where it initiates transcription of several genes, including cochlin (*Coch*), Indian hedgehog (*Ihh*), insulinlike growth factor binding protein 3 (*Igfbp3*), and the immune response gene (*Irg1*) [16–21], but inhibits expression of the homeobox gene *Msx1* [22]. Despite these findings, the LIF-induced attachment cascade, essential for implantation, cannot be explained in toto by the identification of these few isolated factors. Comprehensive knowledge of the repertoire of LIF-induced signaling networks is necessary to understand the complex embryonic attachment process and begin to identify the pathways regulating implantation and cross-talk between the blastocyst, LE, and underlying stroma.

Numerous attempts to identify genes involved in mammalian implantation, some involving genomewide screening

[1]Supported in part by the Singapore Biomedical Research Council and the Singapore Agency for Science, Technology and Research (A*STAR) to C.L.S.
[2]Correspondence: Colin L. Stewart, Developmental and Regenerative Biology, Institute of Medical Biology, A*STAR, 8A Biomedical Grove, #06-06 Immunos, Singapore 138648.
E-mail: colin.stewart@imb.a-star.edu.sg

Received: 11 February 2014.
First decision: 10 March 2014.
Accepted: 23 June 2014.

eISSN: 1529-7268 http://www.biolreprod.org
ISSN: 0006-3363

techniques, have been reported [18, 23–36]. However in most of these studies, gene expression analysis was performed on the entire uterus, either during embryo implantation or between implantation and interimplantation sites following natural mating. While to some extent informative, whole organ approaches exclude the possibility of assigning any change in gene expression to a specific tissue or cell type, or of accurately defining temporal expression patterns. This is particularly important in the case of the LE, which makes up only about 5% of the total number of cells within the uterus [35] and yet is the primary determinant of successful implantation [37].

Here we have confined our analysis of gene expression to the prereceptive LE and at successive time points after LIF treatment. We find that within 3 h, LIF affects the expression of many thousands of genes in the LE, some of which are implicated as being essential for implantation. At least 25 biological process (BP) pathways are altered. We validate the expression profiles and the dynamic cellular localization of selected key genes in 10 pathways: actin cytoskeleton, apoptosis/stress, ephrin receptor, fibroblast growth factor (FGF), insulinlike growth factor 1 (IGF-1), integrin, notch, toll-like receptor, vascular endothelial growth factor (VEGF), and Wnt/β catenin signaling pathways. These findings document the molecular complexity, including the simultaneous activation and repression of multiple signaling pathways that are both transient and dynamic, both transcriptionally and in protein stability, as well as structural alterations in cell organization, adhesion, and associated changes in the extracellular matrix that underlies the switch from a nonreceptive to receptive LE.

MATERIALS AND METHODS

Mice

Mice were maintained at the A*STAR Biological Resource Centre facility and maintained in accordance with the guidelines of the Institutional Animal Care and Use Committee. For the hormone replacement and LIF treatment, 8–10 wk B6C3HF1 mice were ovariectomized (*ovxd*) and rested for 12 days to eliminate endogenous ovarian hormones from the circulation [38]. For three consecutive days, the mice were primed daily with 100 ng of E_2 in sesame oil, rested for 3 days, and then injected with 5 mg Depo-Provera (intraperitoneally) (Pharmacia & Upjohn). After a further 3 days, they were injected with a single dose of 10 μg rLIF (intraperitoneally), a minimum dose previously determined to consistently induce implantation in B6C3HF1 mice [7], euthanized, and uteri recovered at 0, 1, 3, and 6 h after injection. Some females were also sacrificed at 30 min. For the E_2 induction, the animals were prepared in a similar manner except that the LIF injection was replaced with 50 ng E_2.

Isolation of LE

The LE were isolated from the uteri using a modified enzymatic digestion protocol [39]. Uteri were cut into 2 mm pieces and incubated with 1% trypsin (1:250 grade) in HBSS (Invitrogen), pH 7.4 (without Ca^{2+}, Mg^{2+}, or phenol red) at 4°C for 90 min and then room temperature for 1 h and 37°C for 10 min. Trypsin was neutralized with 0.4% soybean trypsin inhibitor with 5 mg/ml DNase1 in HBSS for 5min. The uterine pieces were washed in HBSS and the LE isolated by sliding forceps along the length of the uterine tube. The LE was recovered by gravity sedimentation, washed twice in HBSS, and stored at −70°C in TRIZOL or RLT buffer (Qiagen) prior to RNA extraction. It is estimated that this procedure results in the isolation of LE with ~95% purity [35] because we were unable to detect vimentin mRNA in the isolates, which is a marker for stromal tissue.

Microarray Analysis

Total RNA was extracted (RNeasy; Qiagen) from LE samples. The quality and quantity of total RNA was determined with an Agilent RNA 6000 Nano Kit and Agilent Bioanalyzer 2100. Samples with RNA integrity number (RIN) above 7 were used for microarray analysis, which was performed using MouseWG-6 v2.0 Expression BeadChip (Illumina). Each experimental group consisted of six mice, and each sample (consisting of RNA from a single mouse) was run in duplicate. The samples were randomly assigned to different chips. For the microarray, 500 ng RNA was amplified into cRNA using Illumina TotalPrep-96 RNA Amplification Kit (Applied Biosystems/Ambion) according to the manufacturer's protocol. Amplified cRNA (1.5 μg) was hybridized to each array, and the beads were scanned using BeadArray Reader (Illumina) and analyzed with Genome Studio Software (Illumina).

Microarray Quality Control and Data Analysis

Data from the Genome Studio was imported into the Partek Genome Studio version 6.6. For analysis, quantile normalization was performed on background-subtracted data across all the chips followed by removal of batch effects. Principal component analysis (PCA) monitored the reproducibility of isolation with chip-to-chip and interanimal variations removed. Hierarchical cluster analysis was performed using Pearson dissimilarity correlation coefficient. Three-way analysis of variance (ANOVA) was applied between the different time points with a false discovery rate of 0.05 and a fold change of 1.2. Heat maps, volcano plots, and gene ontology (GO)-enrichment maps were generated from the gene sets obtained from the ANOVA. The gene sets were imported into Ingenuity Pathway Analysis (IPA) (Ingenuity Systems) to identify the canonical pathways. The significance of the association between the data set and the canonical pathway was measured in two ways: 1) as a ratio of the number of molecules from the data set that map to the pathway in relation to the total number of molecules that map to the canonical pathway and 2) using Fisher exact test to calculate a *P* value to determine the probability that the association between the genes in the data set and the canonical pathway is explained by chance alone (www.ingenuity.com company/pdf/Citation Guidelines). For validation of candidate genes from pathways identified by IPA, only those genes in the pathways were considered that showed differences in intensity between the individual groups above 0.275, thereby excluding genes with very low expression levels.

The functional annotation tool available through the Database for Annotation, Visualization and Integrated Discovery (DAVID) (http://david.abcc.ncifcrf.gov/) [40] was used to determine which gene sets were significantly differentially expressed between the 0 and 1 h time points. Transcription factor analysis was performed using the Genomatix MatBase TF software (http://www.genomatix.de/solutions/genomatix-software-suite.html#1) to identify transcription factors altered by LIF at 1 h.

Quantitative Real-Time PCR

Genes identified in the microarray analysis were verified by quantitative real-time PCR (qPCR) using TaqMan (Applied Systems), with HPRT1 acting as an endogenous control with the probe sequences listed (Supplemental Table S1; Supplemental Data are available online at www.biolreprod.org). The CT values for the samples were obtained after baseline correction. Relative fold change or relative expression was calculated by the ΔΔCt method where the expression of the gene of interest is normalized against the endogenous control. The calculated difference (ΔCt) for the experimental time points (1, 3, or 6 h) was subtracted from the control (0 h), resulting in the ΔΔCt value and expressed as relative expression ± SEM. One-way ANOVA with either the Boniferroni parametric or Games-Howell nonparametric test was used for the post hoc analysis and values obtained by comparing the ratio of the expression levels for each sample with the mean of the control samples.

Histology, Immunohistochemistry, and Immunofluorescence

For histological analysis, hematoxylin and eosin staining was performed. Images were viewed and recorded on a Zeiss Axioimager. Immunofluorescence analysis was performed on paraffin-embedded samples. Sections were deparaffinized and rehydrated through a methanol gradient. Antigen retrieval was performed in citrate buffer, pH 6 (Dako), in a 2100 Retriever (PickCell). Sections were incubated in 1% sodium borohydride for 20 min followed by a 10 min wash in PBS, pH7.4, and incubated overnight at 4°C with the primary antibodies (Supplemental Table S2). With the primary mouse monoclonal antibodies, the sections were incubated with Rodent Block M (Biocare Medical) for 20 min to prevent nonspecific binding. Nonspecific antibody binding was blocked by incubation in 10% normal goat serum or 10% donkey serum (Sigma) for 30 min and then washed in PBS. Samples were incubated with 1:500 dilution of secondary Alexa 488 antibodies (Invitrogen) for 1 h and the nuclei labeled with 4′,6-diamidino-2-phenylindole (DAPI), washed in PBS, then in distilled water, and incubated in 50 mM copper sulfate prepared in ammonium acetate buffer, pH 5, for 60–90 min to reduce autofluorescence [41]. The sections were mounted in ProLong gold antifade (Invitrogen) and imaged using a Zeiss LSM510 confocal microscope.

For some sections, endogenous peroxidase was eliminated by incubating the sections in 0.3% H_2O_2 for 30 min. The sections were blocked in 1% normal goat serum (Sigma) in PBS for 30 min and incubated with the rabbit anti-NFkbp65 overnight at 4°C, washed twice in PBS, and incubated in 1:500 diluted biotinylated goat anti-rabbit antibody (Dako) for 30 min at room temperature. After washing, the sections were incubated with streptavidin:biotinylated horseradish peroxidase (ABC; Invitrogen) complex for 20 min followed by PBS rinse and diaminobenzidine and H_2O_2 in PBS for 1–2 min, counterstained with hematoxylin, dehydrated through methanol grades and xylene, and mounted on DPX (Electron Microscopy Sciences).

Western Blot Analysis

Purified LE extract [42] was dissolved in complete Lysis M buffer containing proteinase inhibitor cocktail and 2% SDS (Roche). Protein supernatant (25–40 μg) was electrophoresed in a 4%–15% gradient gel (Bio-Rad) and transferred to polyvinylidene difluoride membrane (PVDF, GE Healthcare), blocked with 5% nonfat dry milk in 25 mM Tris and 0.14 M NaCl containing 0.1% Tween 20 and incubated with their respective antibodies (Supplemental Table S2) prepared in 0.5% nonfat dry milk in the same buffer overnight at 4°C. After a 30 min wash, the Western blots were incubated with 1:10 000 (rabbit) or 1:25 000 (mouse) dilutions of respective secondary antibodies (Dako) for 1 h, then washed and exposed using ECL Prime detection reagent (GE Healthcare). Cyclophilin D and cytokeratin 19 were used as loading controls. Densitometry was performed using the NIH Image J program.

RESULTS

Dynamic Changes in the Uterine Expression of the Estrogen Receptor-α and Progesterone Receptor Following LIF Treatment

The changes in uterine receptivity are driven by a combination of E_2 and P4, acting through their respective receptors, in regulating gene expression in the LE, GE, and stroma. Because we omitted nidatory E_2 in initiating the change in receptivity, it was necessary to first determine whether the substitution of E_2 by LIF affects the estrogen receptor-α (ESR) and progesterone receptor (PGR) distribution because they function as key transcription and cotranscription factors in the different uterine compartments.

A previous study indicated that on D4, ESR expression was high in the GE, with lower levels in the LE and subepithelial stroma [43]. By D5, increased ESR expression is detected in the GE, LE, and stroma. We compared ESR expression in the uteri at successive time points after treating the *ovxd* mice either with 50 ng of E_2 or 10 μg LIF (Fig. 1, A and B). In the GE, at 0 h, ESR was detected in a few glands and cells in the adjacent stroma (Fig. 1Aa–Ae). E_2 induced a strong ESR signal in the GE within 1 h after injection (Fig. 1Af). The levels increased, together with the ESR localizing to the GE nuclei at later time points (Fig. 1, Ag and Ah). In the LE, ESR expression was detectable at 1 h, although predominantly cytoplasmic and at the apical edge (Fig. 1Ab). However, by 3 h, many LE and subepithelial stromal cells showed a nuclear localization of the ESR (Fig. 1, Ac and Ag). LIF treatment resulted in a similar pattern of ESR induction, however at both a slower rate and at a lower intensity, with more intense expression being detected in the LE and GE only at 6 h after LIF treatment (Fig. 1, Bd and Bh).

PGR was detected primarily in the LE and subepithelial stroma, with little if any in the GE on D4. By D5, PGR expression was restricted to the subepithelial stroma [43]. In the LIF-treated mice, a similar pattern of PGR expression was noted, with strong localization of PGR to the LE at 0 h and weak expression in the subepithelial stroma (Fig. 1, Ca and Ce). At 1 h, PGR expression transiently declined in the LE (Fig. 1Cb), but by 3 h, expression had intensified in the LE and subepithelial stroma, a pattern that persisted to 6 h (Fig. 1, Cc, Cd, Cg, and Ch). Little or no PGR expression was detected in the GE at any time (Fig, 1, Ce–Ch). These observations indicate that LIF-initiated changes in LE gene expression in the first 3 h are probably independent of the ESR, with the PGR being predominately localized to the LE, albeit in a dynamic manner, due to the transient decline within the LE within the first hour after LIF, though strong PGR expression is restored in the LE and stroma by 3 h after LIF.

LIF Initiates Nuclear pSTAT3 Translocation in the LE but Not GE

In the LE, LIF stimulates the JAK-STAT transcription pathway, culminating in the activation and nuclear translocation of the transcription factor STAT3 [13]. Immunofluorescence analysis revealed that both the LIFR and gp130 were expressed in the LE and GE (Fig. 2, A and B). At 0 h, the LIFR localized to the apical and basal membranes of the LE, with lower levels of expression in the basal membranes of the GE (Fig. 2Aa). By 1 h, signal intensity had markedly increased in the LE and GE (Fig. 2Ac). Thereafter, the signal intensity declined to a minimal level in the LE by 6 h (Fig. 2Ae). Total LIFR expression confirmed the decline at 3 and 6 h (Supplemental Fig. S1A). The gp130 was detectable on the LE apical membrane at 0 h (Fig. 2Ba). The signal intensity subsequently increased with a maximal intensity at 3 h before declining to minimal levels by 6 h (Fig. 2, Bb–Be). To confirm that the LE responded to LIF, we examined STAT3 activation. Nonphosphorylated STAT3 was detected in the cytoplasm at 0 h, consistent with previous results [13] (Fig. 2Ca). By 1 h expression of pTyr-STAT3 increased (as measured by pTyr-STAT3-specific antibodies) with translocation into the majority of the LE nuclei (Figs. 2Cd and Supplemental Fig. S1B). By 3 h, pTyr-STAT3 levels declined, and STAT3 was no longer concentrated in the nuclei (Fig. 2Ce). Interestingly, the GE, which in the mouse synthesizes LIF, may not apparently respond to LIF, as indicated by the absence of nuclear pSTAT3, despite pSTAT3 protein being detected in the cytoplasm of the GE at all the time points (Fig. 2D). In the stroma, nuclear pSTAT3 was observed in a few isolated cells and the vascular endothelium (Figs. 2, C and D). In contrast, STAT5B, which is also induced by E_2 in the uterus [44], was identified in only a few stromal cells at any time (data not shown).

LIF Initiated Changes in LE Gene Expression

To determine the changes in gene expression initiated by LIF, we performed a comparative array analysis on total RNA isolated from the LE at successive time points. PCA and ANOVA-based Partek analysis were used for the statistical assessments. PCA revealed that all the samples at each specific time point were tightly clustered; indicating a high level of reproducibility across at the different times (Supplemental Fig. S2A). Hierarchical clustering analysis further identified two distinct expression patterns: 1) between 0 and 1 h and 2) between 3 and 6 h (Supplemental Fig. S2B). The overall expression profile at 6 h was closer to that at 0 h (i.e., untreated) than to the 1 h time point.

We first analyzed whether known LIF-regulated genes underwent expected changes in expression (Supplemental Fig. S3, a–f). Based on previous reports, *Coch, Igfbp3, Msx1, Irg1,* and *Ihh* are regulated by LIF in the LE [18, 19, 21, 22, 45, 46], although *Ihh* is also regulated by PGR receptor [47]. Our microarray data reflected the same changes in the expression of these genes: *Coch, Igfbp3, Irg1,* and *Ihh* all increased

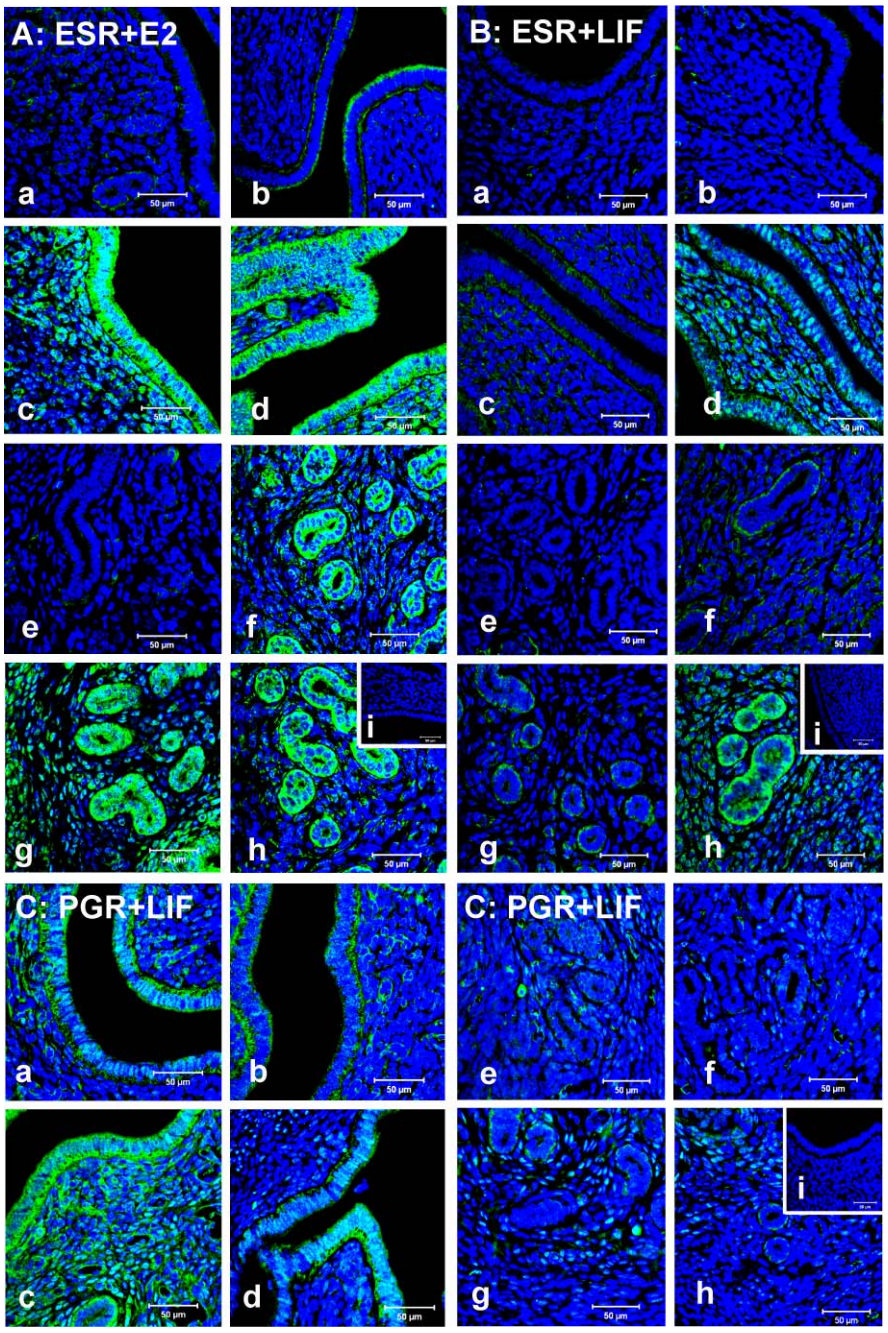

FIG. 1. Estrogen (ESR) and progesterone (PGR) receptor expression and localization change in response to LIF. **A**) ESR (green) uterine expression after E_2 treatment (**a**: 0 h; **b**: 1 h; **c**: 3 h; **d**: 6 h; **i**: negative control) increased levels and nuclear localization of ESR in the LE and stroma by 3 and 6 h posttreatment. In the GE, ESR expression is activated by 1 h (**e**: 0 h; **f**: 1 h; **g**: 3 h; **h**: 6 h). Bar = 50 µm. Nuclei (blue) are stained with 4′,6-diamidino-2-phenylindole. **B**) ESR (green) expression after LIF injection (**a**: 0 h; **b**: 1 h; **c**: 3 h; **d**: 6 h; **i**: negative control) reveals nuclear localization of ESR in the LE and stroma by 6 h. ESR was not strongly induced till 6 h, and nuclear localization was not seen in the GE (**e**: 0 h; **f**: 1 h; **g**: 3 h; **h**: 6 h). Bar = 50 µm. **C**) PGR (green) expression after LIF injection (**a**: 0 h; **b**: 1 h; **c**: 3 h; **d**: 6 h; **i**: negative control) identified nuclear PGR at 0 h in the LE. By 1 h, LIF caused a reduction in PGR expression in the LE and nuclei, after which it substantially increases in the LE and stroma by 3 h. PGR expression in the stroma falls by 6 h. No change in PGR expression or localization was seen in the GE within 6 h of LIF (**e**: 0 h; **f**: 1 h; **g**: 3 h; **h**: 6 h). Bar = 50 µm.

(Supplemental Fig. S3, Aa, Ab, and Ad–Af), while *Msx1* declined in response to LIF (Supplemental Fig. S3Ac). We confirmed the change in expression of *Coch*, *Irg1*, and *Msx1* by qPCR (Supplemental Fig. S3, Ba–Bc). *Coch* levels increased by 6 h, and *Irg1* increased by 3 h, after which its expression declined (Supplemental Fig. S3, Ba and Bb). In contrast, *Msx1* levels transiently increased at 1 h but by 6 h had declined to a level lower than that before LIF treatment (Supplemental Fig. S3Bc). Genes such as interleukin-1 alpha (*Il1α*) and oncostatin M (*Osm*), which are expressed in the LE and stroma at implantation [48, 49], although detectable at basal levels, were not altered by LIF treatment (data not shown). Other LE-restricted genes, including cyclooxygenase 1 (*Ptgs1*, also known as *Cox1*) [50] and lipocalin 2 (*Lcn2*), were analyzed. *Ptgs1* expression fell at both the mRNA and protein levels (Supplemental Fig. S4, A, B, Ca, and Cb). COX-1 protein was expressed predominantly at the perinuclear boundary in cells of the LE. Similarly, transcript expression of *Lcn2*, an acute-phase

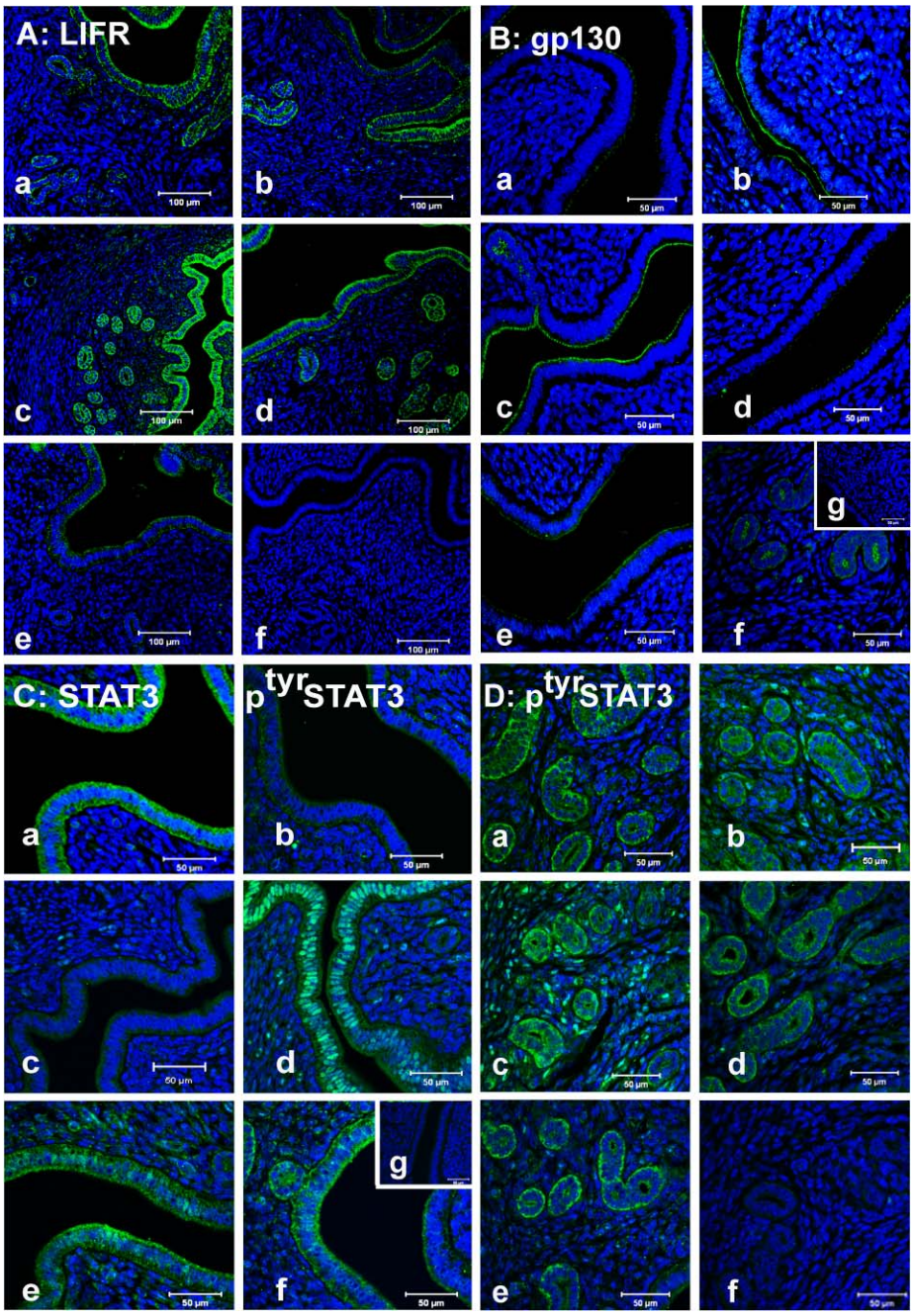

FIG. 2. LIF stimulates the JAK-STAT pathway resulting in nuclear translocation of pSTAT3 in the LE but not GE. **A**) LIFR expression (green) increases in the LE and GE within 1 h of LIF injection (**a**: 0 h; **b**: 30 min, **c**: 1 h; **d**: 3 h; **e**: 6 h; **f**: negative control). Bar = 100 μm. **B**) The gp130 (green) increases by 1 h at the apical surface of the LE (**a**: 0 h; **b**: 30 min, **c**: 1 h; **d**: 3 h; **e**: 6 h; **g**: negative control). Expression of gp130 in the GE at 1 h is shown in **f**. Bar = 50 μm. **C**) Nonphosphorylated Stat3 is abundant in the LE cytoplasm at 0 h (**a**). Nuclear translocation of phospho^{tyr705}STAT3 (green) occurs in the LE at 1 h after LIF injection (**b**: 0 h; **c**: 30 min, **d**: 1 h; **e**: 3 h; **f**: 6 h; **g**: negative control). Bar = 50 μm. **D**) The GE does not respond to LIF even though STAT3 is present in the GE cytoplasm as revealed by the lack of p-STAT3 (green) localization to the nuclei, despite the presence of LIFR and gp130 in the GE (**a** 0 h; **b**: 30 min, **c**: 1 h; **d**: 3 h; **e**: 6 h; **f**: negative control). Bar = 50 μm.

protein expressed by the LE and GE and regulated by E_2, increased at 3 and 6 h (Supplemental Fig. S4D) [51]. This was contrary to a previous report where *Lcn2* declines in response to nidatory E_2 [35]. Genes expressed in the stroma, such as vimentin and desmin, remained at basal levels and were unaltered by LIF treatment (data not shown) [52]. These changes in gene expression demonstrate that the LE responds to LIF to the same extent seen in normal uteri on D4 following nidatory E_2.

The array data was then subjected to a three-way ANOVA. A 1.2-fold change allowed us to identify specific gene networks in the LE and the dynamics of their expression over the 6 h following LIF treatment. The volcano plots obtained by comparison analysis of the data revealed that within 1 h of LIF administration 489 genes exhibited altered expression (144 reduced versus 345 increased). By 3 h, this had increased to 3987 genes, but by 6 h, the number had marginally decreased to 3651 (Supplemental Fig. S2, Ca–Cc, respectively). Heat

maps also illustrated the overall changes in gene expression at the different time points (Supplemental Fig. S5).

GO (http://www.geneontology.org) annotation, DAVID bioinformatics database, and IPA were used for the categorization and deep analysis of the gene lists. Deep analysis of LIF-induced changes focused on the BP category. Within 1 h of treatment, the largest BP categories of the 487 genes identified were immune response, blood vessel/vascular development, regulation of cell proliferation, and transcriptional regulation (22.12%). By 3 and 6 h, the dominant LIF-initiated BP categories were cellular metabolic processes, cellular component and complex subunit organization, together with the synthesis of biopolymers, macromolecules, carbohydrates, and lipids (38.58% and 42.13% at 3 and 6 h, respectively). Induction of stress response and cell death were also significantly induced BPs (11.74% and 7.47% at 3 and 6 h, respectively). The genes associated with each of the BPs are listed in Supplemental Table S3.

Changes in LE Gene Expression in the First Hour after LIF Injection

We reasoned that changes occurring during the first hour were likely to be those involved in making the LE receptive to blastocysts as well as those involved at initiating stromal decidualization, that is, defining which genes maintain the refractory/prereceptive state and those associated with the onset of the receptive state in direct response to LIF-STAT3. From the list of genes, after removing all RIK, LOC, and unknown transcripts, 54 annotated genes with reduced expression were identified (Supplemental Table S4). These genes were submitted to the DAVID Bioinformatics Database for GO analysis to identify gene clusters common to biologically related themes [40]. Full analyses and lists of enriched annotation terms for the gene groups can be found in Supplemental Table S5.

GO analysis categorized the genes into intermediate filament-cytoskeletal organization, which included the keratins (K5, 14, 15, 17), collagen 17A1, cofilin-1, claudin 5, kinesin C2, and Arc. Chromatin organization was another GO pathway associated with reduced expression of two genes, *Cbx8* and *Suv420H2,* which maintain pericentric heterochromatin, as well changes in the histone clusters HIST1H4K and HIST4H4. Two previously characterized transcription factors, ERRFI1/MIG-6, required for P4 inhibition of E_2-mediated proliferation, and *Cited2*, which functions as a PRG-regulated trans-activator for Cbp/p300, were also reduced in the LE. Intriguingly, two genes involved in regulating circadian rhythmicity, *Per1* and *RGS16,* showed reduced expression, with *Per1* having been previously reported as a PGR-regulated gene in the uterus [53] (Supplemental Table S5).

Within 1 h, 256 genes/transcripts (excluding RIK and LOC sequences) were induced in the LE. The GO BPs that were induced included inflammatory/innate immune responses (*Cxcl1, NfKBIZ, Selp, Ccl2, Cfb, C3, Sphk1, Saa3, SerpinG1, STAT3, Ccl7, Cxcl10, SerpinA3N, Nupr1, Igbp4, F2R*) and vascular development/angiogenesis (*Sox17, Ihh, Notch, Hey2, endothelin 1*). Significantly, there was increased expression of 42 transcription factors, including *Sox 7, 9,* and *17, Cebp/β, HoxD10, HoxB4 and B10, Hes1, Hey1 Nfkβ, Bcl3, Kfl 6* and *9*, and *Rel* genes (Supplemental Tables S4 and S6).

LIF Induces a Diverse Repertoire of Networks in the LE

IPA revealed that more than 30 pathways were altered by LIF treatment across all the time points. Eighteen pathways at each time point were selected (Supplemental Fig. S6). These included the JAK-STAT, IGF-1, VEGF, Sonic Hedgehog, Wnt/β-catenin, ephrin, Notch, and TGF-β pathways, metabolic pathway mTOR, cytoskeletal pathways affecting actin organization, integrin receptor β activation, innate immunity/inflammation and vasculogenesis, such as stress response/apoptosis, and Toll-like receptor (TLR) pathways. To confirm the authenticity of the microarray results, we validated the dynamics in the expression of selected proteins from 10 of these pathways of which a selection are described in detail below.

IGF1 Pathway

In the LE, IGF1 receptor (IGF1r) mediates E_2-induced cell proliferation [54, 55]. Over the 6 h period, components of the IGF1 pathway underwent an initial increase followed by a decrease in expression. These included *Igf1r,* insulinlike growth factor-binding proteins 3, 4, and 6 (*Igfbps3, 4,* and *6*), glycogen synthase kinase 3 beta (*Gsk3*β), and cysteine-rich, angiogenic inducer, 61 (*Cyr61*). The expression of *Igf1r* and *Igfbp3* was validated by qPCR, Western blot, and immunofluorescence analyses. The transcript levels of *Igf1r* and apical membrane expression of phospho^{tyr} IGF1r protein were reduced at 3 and 6 h (Fig. 3, Ac and Ad, and Supplemental Fig. S7Ac). Intriguingly, a nuclear form of this protein was apparent [56] that increased at 1 and 3 h, after which its expression declined (Fig. 3, Ab, Ac, and Ae). In line with previous reports, IGFBP3 was induced by LIF [19], with transcript and protein levels increased by 3 h (Fig. 3Bc and Supplemental Fig. S7, B and C). Although the IGF1 pathway regulates epithelial proliferation prior to implantation, we did not detect any increase in the proliferation marker Ki67 within the 6 h following LIF treatment (data not shown). However, at 1 h, cyclinD1 (a marker for proliferating LE [57]) transiently localized to the LE nuclei (Fig. 3Cb), at the same time as nuclear localization of the PGR fell (Fig. 1Cb), whereas at 0, 3, and 6 h, cyclinD1 was primarily cytoplasmic. Based on the reduction in membrane-associated IGF1R, its translocation to the nucleus along with increased IGFBP3, which sequesters the IGFs, it would appear that LIF inhibits IGF1 signaling in the LE.

LIF treatment reduced the levels of phospho^{tyr1161}IGF1R at the LE cell surface with concurrent translocation to the nucleus. Although the IGF1R lacks nuclear localization signals, nuclear translocation of this receptor has been noted in tumor cells, where IGF1R associates with the WNT-regulated transcription factor LEF1 [58, 59]. Together these factors increase the levels of cyclin D1 and AXIN2 [56]. Whether nuclear IGF1R has similar functions in the LE remains to be determined.

VEGF Pathway

The first overt indication of the start of implantation is an increase in uterine vascular permeability leading to edema. Following blastocyst invasion, the uterus undergoes extensive vascular remodeling to support stromal decidualization. Vascular remodeling is regulated by a variety of growth factors, particularly the VEGFs, FGFs, and platelet-derived growth factors(PDGFs); antibody-mediated inhibition of VEGF alone is sufficient to block implantation [60].

The VEGF family consists of five genes ($VEGFA_{164}$, B, C, and D, and PLGF) with each gene generating many different isoforms [61]. Although *Vegf-a* is the predominant form in the LE and is primarily responsible for stimulating angiogenesis, its expression was unaltered by LIF (data not shown). *Vegf-b*,

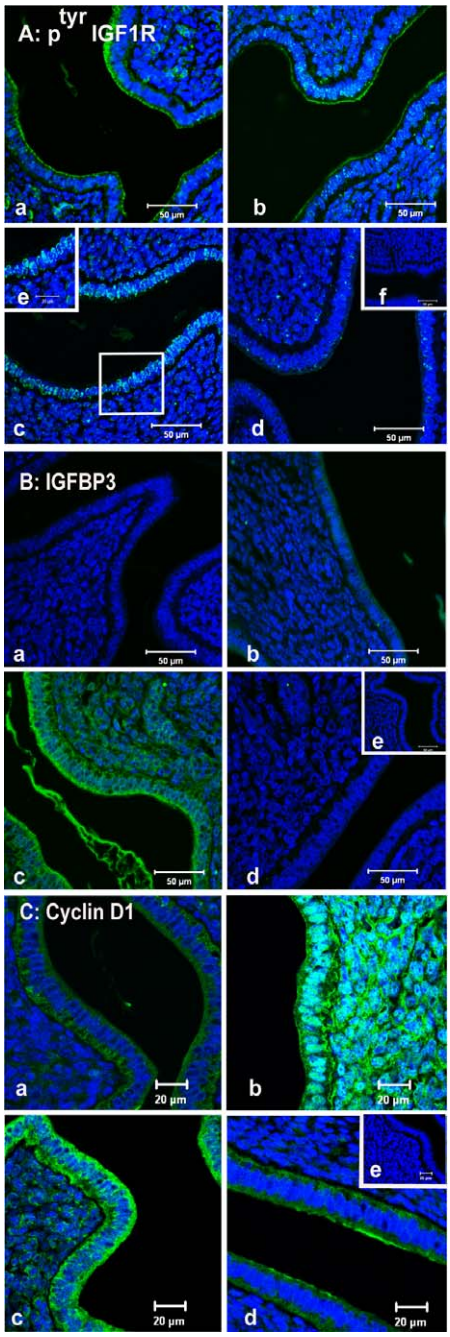

FIG. 3. LIFs effects on the insulinlike growth factor-1 receptor pathway. **A**) Phospho^{tyr1161}IGF1R (green) localization following LIF is reduced at the apical LE membranes (**a**: 0 h; **b**: 1 h; **c**: 3 h; **d**: 6 h; **f**: negative control). There is an increase in a novel nuclear form of Igf1R in the LE nuclei at 1 and 3 h (**e**). Bars for **a**, **b**, **c**, **d**, **f** = 50 μm and for **e** = 20 μm. **B**) IGFBP3 (green) increases following LIF (**a**: 0 h; **b**: 1 h; **c**: 3 h; **d**: 6 h; **e**: negative control) by 3 h. Bar = 50 μm. **C**) Cyclin D1 (green) shows transient nuclear localization at 1 h following LIF treatment in the LE (**a**: 0 h; **b**: 1 h; **c**: 3 h; **d**: 6 h; **e**: negative control). By 3 h, Cyclin D1 had relocated to the cytoplasm. Bar = 50 μm.

which is required for blood vessel survival/maintenance, increased at the transcript level at 3 h after which levels declined (Supplemental Fig. S8A). Levels of VEGFB protein in the LE declined by 1 h and continued to do so in the ensuing 6 h (Fig. 4A and Supplemental Fig. S8, Ba and Bb), although by 1 h VEGFB stromal expression significantly increased (Fig. 4Ab). Of the VEGF receptors, expression of VEGFR1 (FLT-1), which binds VEGFA and B, was unchanged in the LE until 3 h, where it localized at the apical surface, followed by more intense expression in the subepithelial stroma at 6 h (Fig. 4Cd). VEGFR2 (FLK-1) binds VEGFs A and C–E, and its expression became more obvious in the LE and stromal blood vessels by 1 h (Fig. 4Cb). By 3 h, VEGFR2 was showing marked nuclear accumulation in the LE and in many cells in the stroma (Fig. 4Cc) [62], but by 6 h, expression had declined (Fig. 4Cd). VEGFR3 (FLT4), which regulates lymphangiogenesis, appeared to be weakly expressed in the LE apical membranes and GE throughout the 6 h time frame without any overt changes in expression (data not shown).

From the array data, expression of the hypoxia inhibitory transcription factor 1α (HIF1α), which regulates VEGF expression [63], was initially high but had fallen by 6 h. HIF1α protein was localized in the LE nuclei at 0 and 1 h, with a marked increase in the stromal nuclei appearing by 1 h (Fig. 4, Da and Db). By 3–6 h, nuclear localization in the LE had declined, and by 6 h, overall levels in both the LE and stroma had declined (Fig. 4, Dc and Dd). There was some relocalization of HIF1α from the nucleus to cytoplasm at 3 h (Fig. 4Dc). Overall, the relative paucity in changes in the different components of the VEGF family of ligands/receptors in response to LIF suggests that the implanting blastocyst may be the prime inducer of the VEGF network. Nevertheless, it is intriguing that in the retina and other tissues, LIF appears to inhibit VEGF, HIF-1 expression, and microvessel formation [64].

TLR Signaling

The interleukin-1 receptor/TLR system (IL1r/TLR) is a key component of the innate immune system (IIS) and is the first line of the host defense system against infectious microorganisms. In mammals, bacterial lipopolysaccharide stimulates the IIS by binding to the receptor complex consisting of CD14, MD2, and TLR4. This receptor complex activates the *MyD88* (myeloid differentiation factor 88) pathway by recruiting the myeloid differentiation primary response gene 88 (*Myd88*) and culminating in activation of the NFκB and MAPK transcription factors [65]. These then induce the production of proinflammatory cytokines, such as TNFα and IL-1 and -6. From the array data, genes altered in this pathway were lipopolysaccharide-binding protein (*Lbp*), the TLR 1, 2, and 4 (*Tlr1, Tlr2*, and *Tlr4*), CD14 (*Cd14*), *Myd88,* and ECSIT homolog (*Ecsit*). The data revealed significant activation of the Toll pathway by 3–6 h. Expression of TLR2 and CD14, a coreceptor for TLR4, were further validated, with transcripts for *Tlr2* increasing by 3 h and then declining by 6 h (Supplemental Fig. S9A), while TLR2 protein localized to the cell membrane and cytoplasm of the LE (Fig. 5A), as previously reported [35, 66]. The expression of TLR2 protein in the LE prior to LIF stimulation was minimal, with a slight increase being noted by 3 h (Fig. 5Ab–Ad). In the stroma, robust protein expression of TLR2 and CD14 was evident by 3 h (Fig. 5, Ac and Bc), possibly due to soluble protein diffusing from the LE to the stroma (Fig. 5, Ab and Ac) because CD14 transcripts are only present in the LE [35]. Alternatively, TLR2 and CD14 stromal expression may be due to some secondary signal, induced by LIF in the LE, transiently stimulating expression of these factors. Total membrane and soluble protein levels for TLR2 fell by 6 h (Supplemental Fig. S9, Ba–Bc). CD14 protein was detected both on LE membranes and in the cytoplasm (Fig. 5B), in agreement with a previous report based on mRNA in situ analysis [35]. By 3 h, the expression increased, but by 6 h, CD14 levels had fallen (Fig. 5B and Supplemental Fig. S9, C, Da, and Db). As with

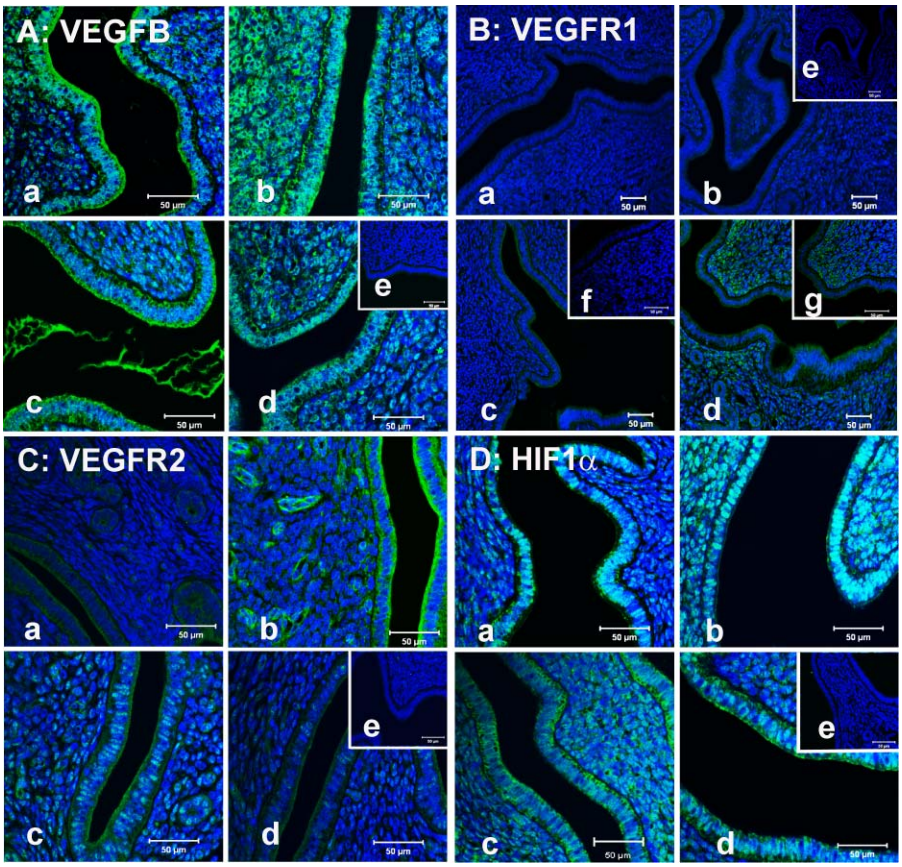

FIG. 4. VEGF pathway alterations induced by LIF. **A**) VEGFB (green) (**a**: 0 h; **b**: 1 h; **c**: 3 h; **d**: 6 h; **e**: negative control) increases at 3 h**.** Bar = 50 μm. **B**) VEGFR1/FLT-1 (green) (**a**: 0 h; **b**: 1 h; **c**: 3 h; **d**: 6 h; **e**: negative control) increases in the subepithelial stromal cells at 6 h**.** Higher magnification images at 3 and 6 h are shown in **f** and **g**, respectively. Bar = 50 μm. **C**) VEGFR2/FLK-1 (green) (**a**: 0 h; **b**: 1 h; **c**: 3 h; **d**: 6 h; **e**: negative control) increases in the LE and stromal blood vessels at 1 h and nuclear localization in LE and stroma at 3 h**.** Bar = 50 μm. **D**) The HIF 1α transcription factor declines by 6 h (**a**: 0 h; **b**: 1 h; **c**: 3 h; **d**: 6 h; **e**: negative control). Bar = 50 μm.

TLR2, we observed increased CD14 levels at 1 and 3 h in the stroma (Fig. 5, Bb and Bc).

Induction of all these changes is initiated in the absence of embryos, suggesting that the presence of the embryo in the uterus is, at some level, anticipated. However, it seems unlikely that the immune response is essential to the switch in receptivity as deletion or inhibition of some key components of the immune response (e.g., *Cd14, Il1r,* and *Coch,* which has bacteriostatic properties [67]) has little or no effect on implantation rates in mice [18, 68, 69].

Stress Response/Apoptosis Signaling

In parallel with the activation of the TLR pathway, we characterized the activation of stress response/apoptosis pathways. The *RelA* viral oncogene, B-cell CLL/lymphoma 2, 3, and 6 (*Bcl2, 3,* and *6*), nuclear factor of kappa light chain gene enhancer in B-cells inhibitor, alpha (*Nfkbi*α) or I-kappa-B-alpha (*IκBα*), *Fas* (TNF receptor superfamily, member 6), BCL2-antagonist/killer 1 (*Bak1*), BH3-interacting domain death agonist (Bid), lamin A (*Lmna*), nuclear factor of kappa light polypeptide gene enhancer in B-cell inhibitor, beta (*Nfkbi*β), tumor necrosis factor receptor, member 1B (*Tnfrsf1*β), and tumor necrosis factor receptor, member 1A (*Tnfrsf1*α) were induced. Three genes—*RelA*, *Bcl3,* and *Nfkbi*α—were further validated. The levels of all three transcripts increased by 3 h, after which they declined (Supplemental Fig. S10, A, E, and F). Nfκbp65 transcript and protein levels were confirmed by Western blot analysis and immunofluorescence (Supplemental Fig. S10, C, Da, and Db). Cytoplasmic localization of total NFκBp65 increased at 3 h and peaked at 6 h in the LE (Supplemental Fig. S10B).

Actin Cytoskeleton Organization

The morphology of the LE changes during implantation in rodents, particularly in organization of the subapical actin network, lateral membrane tight junctions, and persistence of pinopod/microvilli [70, 71]. LIF induces many changes in the LE apical actin cytoskeletal network (Supplemental Fig. S11A–E). Prominent genes affected in this network included beta actin (*Actn*β*)*, breast cancer anti-estrogen resistance 1 (*CAS*) (*Bcar1*), p21 protein (Cdc42/Rac)-activated kinase 3 (*Pak3*), profilin 1 (*Pfn1*), profilin 2 (*Pfn2*), PTK2 protein tyrosine kinase 2 (*Ptk2*), moesin (*Msn*), and actin-related protein 2/3 complex, subunit 1B (*Arpc1*β). Furthermore, two genes, *Shroom3* and *Nuak2,* that induce stress fiber formation and apical constrictions during epithelial invagination increased by 1 h. We validated the changes in expression of *Actn1*, *Actn*β, and *Bcar1* by qPCR. *Actn1* transcripts increased at 3 h and then declined by 6 h (Supplemental Fig. S11A), while expression of *Actnb* and *Bcar1* transcripts increased at 1 h (Supplemental Fig. S11, B and C) and then fell. β-Actin localized to the apical surface of the epithelium, but this localization declined by 3 h (Fig. 6, Ab and Ac). Protein levels

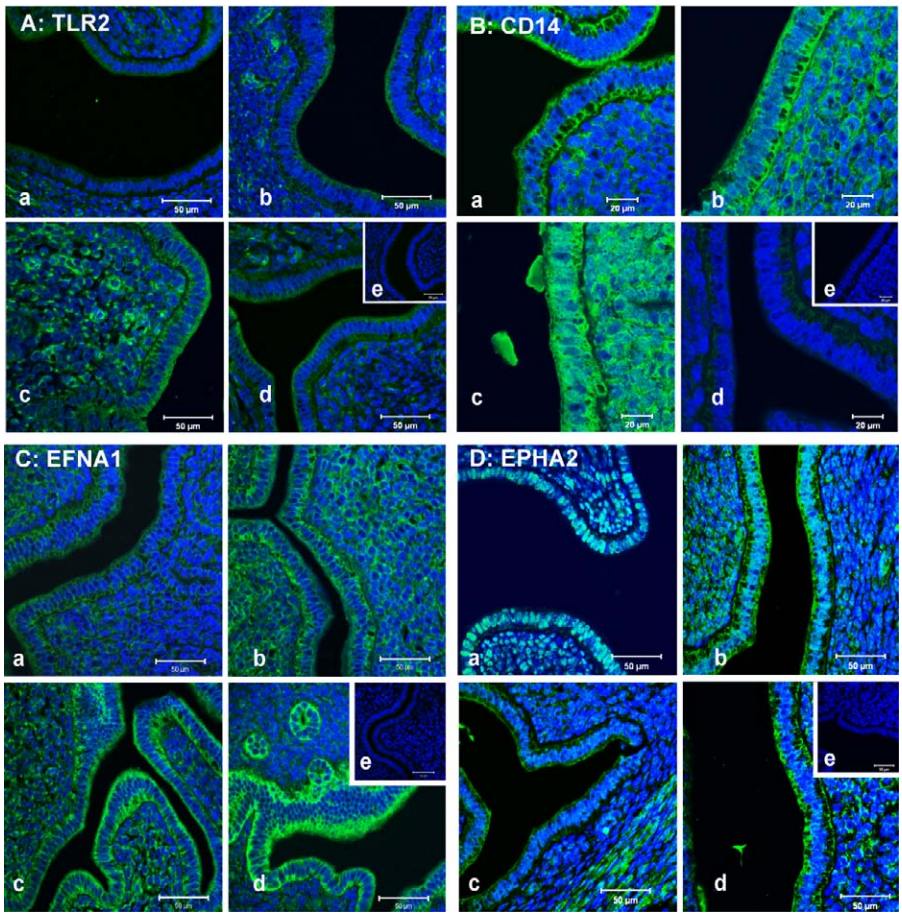

FIG. 5. The innate immune response and ephrin receptor pathways are modulated by LIF. **A**) Membrane expression of TLR2 (green) in the LE peaks at 3 h after LIF (**a**: 0 h; **b**: 1 h; **c**: 3 h; **d**: 6 h; **e**: negative control) as does stromal TLR2 expression. Bar = 50 μm. **B**) CD14 (green) increases in both the LE and stroma at 1 and 3 h (**a**: 0 h; **b**: 1 h; **c**: 3 h; **d**: 6 h; **e**: negative control). Bar = 20 μm. **C**) Ephrin A1 (green) increases in the LE. Stromal expression also increases at 1 and 3 h. (**a**: 0 h; **b**: 1 h; **c**: 3 h; **d**: 6 h; **e**: negative control). Bar = 50 μm. **D**) Membrane localization of EPHA2 (green) initially increases at 1 h, then declines, and then further increases at 6 h (**a**: 0 h; **b**: 1 h; **c**: 3 h; **d**: 6 h; **e**: negative control). Bar = 50 μm.

of β-actin showed a steady decline by 3 and 6 h (Supplemental Fig. S11, Da and Db).

The cell surface adhesion molecule, E-Cadherin (CDH1) is essential for formation and development of the uterine epithelium. Deletion of E-Cadherin in the neonatal uterus leads to infertility due to a failure in endometrial gland formation [72]. Although E-Cadherin was not identified as a LIF-regulated gene in the array analysis, it did undergo significant redistribution in the LE, becoming largely restricted to the apical surface, with lower levels in the basal and lateral membranes, in agreement with previous observations (Fig. 8D) [73].

Eph/Ephrin Receptor Pathway

Few studies have reported on the potential role of the Ephrin pathway in regulating uterine function/blastocyst implantation. This is somewhat surprising because Eph/ephrin signaling is important in regulating cell-cell interactions, including cell repulsion, attraction, and migration, during embryonic segmentation and angiogenesis [74]. One study indicated decreased expression of EPH-A2 in the murine LE during implantation [75], whereas in the human endometrium, EPH-A2 appeared to be abundant during the proliferative phase compared to the secretory phase of the cycle [76] and *Eph-A1*-null mice have abnormal uterine development [77]. Our analysis indicated a general elevation in expression of components of the *Eph* pathway at 3 h followed by reduced levels by 6 h. Genes whose expression changed were: ephrin A1 (*Efna1*), ephrin A5 (*Efna5*), ephrin receptor A2 (*EphA2*), ephrin receptor B2 (*Ephb2*), v-Ki-ras2 Kirsten rat sarcoma viral oncogene homolog (*Kras*), syndecan binding protein (syntenin) (*Sdcbp*), and LIM domain kinase 1 (*Limk1*). Validation of mRNA expression levels of the ligand *Efna1*, the receptor *EphA2,* and the intermediate gene, *Kras,* was performed. The proangiogenic ephrin *Efna1* transcript levels increased over 6 h (Supplemental Fig. S11A). At 0 h, EFNA1 protein localized to the basal cell membrane of the LE (Fig. 5Ca) with expression subsequently increasing. By 1 h, it was also transiently present in the stroma (Fig. 5, Cb and Cc) with stromal expression declining and LE expression increasing by 6 h (Fig. 5Cd).

Ephrin receptor A2 (Epha2), the receptor for EFNA1, underwent dynamic changes in its subcellular localization. At 0 h, EPHA2 concentrated intensely at the perinuclear envelope (Fig. 5Da). By 1 h, signal intensity increased and the receptor redistributed to the cell membrane (Fig. 5Db). At 3 h, the expression decreased at both the membrane and perinuclear regions followed by a slight increase at 6 h at the basal and apical LE membranes (Fig. 5, Dc and Dd). Transcript levels either did not change or declined slightly (Supplemental Fig. S11C). *Kras* transcripts had increased at 1 h and subsequently fell (Supplemental Fig. S11D).

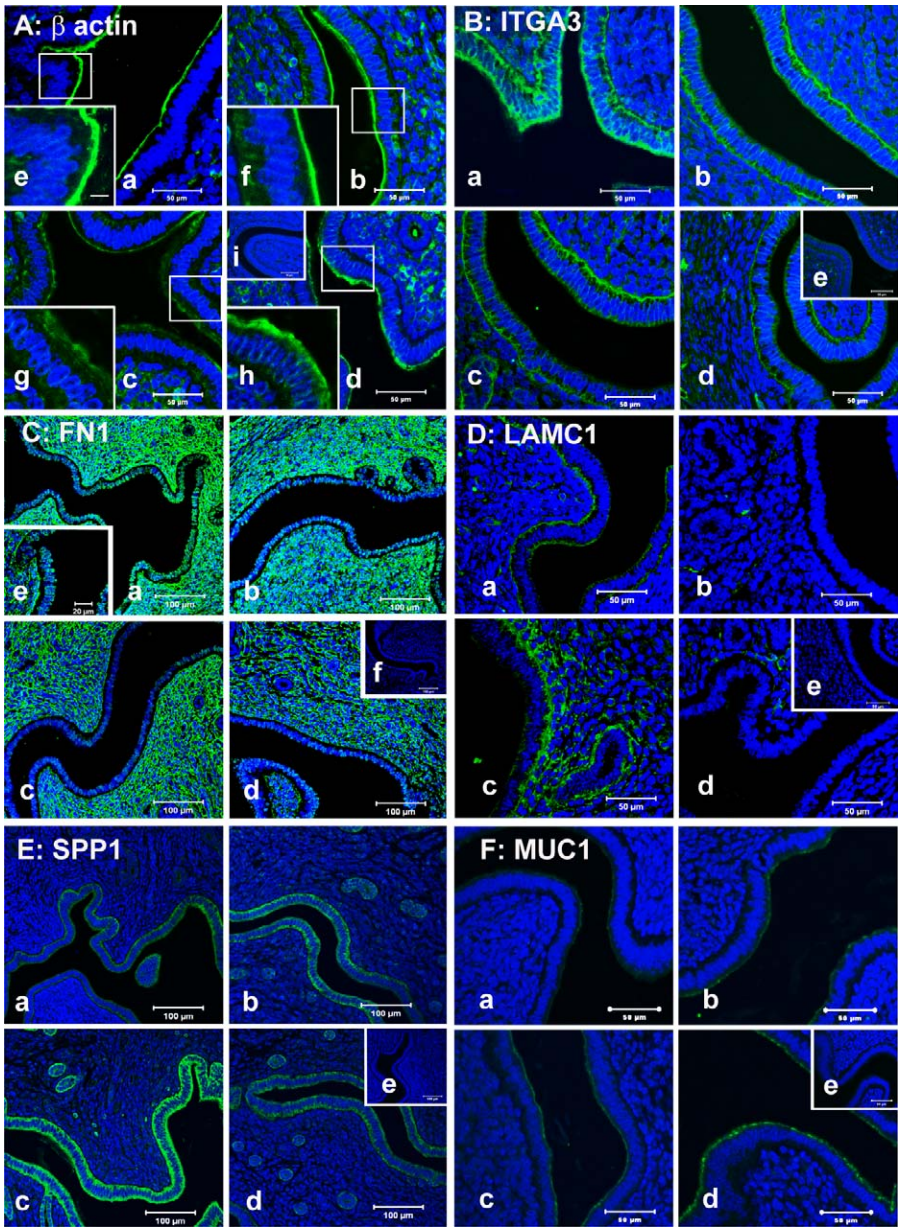

FIG. 6. LIF induced changes in actin cytoskeleton organization, integrins, and extracellular matrix components in the LE. **A**) β-Actin immunostaining (green) (**a**: 0 h; **b**: 1 h; **c**: 3 h; **d**: 6 h; i: negative control) suggests a reduction in β-actin levels underlying the apical LE membrane at 1 and 3 h. The subpanels **e**, **f**, **g**, and **h** are magnified images of the boxed areas shown in subpanels **a**, **b**, **c**, **d**. Bar = 50 μm. **B**) ITGA3 (green) expression declines at the LE apical membrane (**a**: 0 h; **b**: 1 h; **c**: 3 h; **d**: 6 h; e: negative control). Bar = 50 μm. **C**) Fibronectin 1 (green) expression declines in the LE and stroma by 3 and 6 h (**a**: 0 h; **b**: 1 h; **c**: 3 h; **d**: 6 h; **e**: negative control) . Bar = 100 μm. **D**) Laminin C1 (green) declines but then transiently increase in the sub-LE stroma at 3 h (**a**: 0 h; **b**: 1 h; **c**: 3 h; **d**: 6 h; **e**: negative control). Bar = 50 μm. **E**) Osteopontin (SPP1) (green) expression increases in the LE at 3 h (**a**: 0 h; **b**: 1 h; **c**: 3 h; **d**: 6 h; **e**: negative control). Bar = 100 μm. **F**) MUC1 (green) expression in the LE progressively increases by 6 h (**a**: 0 h; **b**: 1 h; **c**: 3 h; **d**: 6 h; **e**: negative control). Bar = 50 μm.

Ephrin A1 activation also results in STAT3 phosphorylation in myotubes [78], and there is evidence that in gastric cancer STAT3 binds to the *Tlr2* promoter to drive cell survival, proliferation, and suppression of apoptosis [79]. The increased LE levels of ephrinA1 and STAT3 within 1 h of LIF administration suggest an association between the two events. Similar to the human endometrium, the ephrin A1 system might be involved in reduction of the cell-to-cell integrity in the LE [75]. Ephrin A1 can also modulate integrin function by dephosphorylating focal adhesion kinase (FAK) and paxillin [80]. BCAR1/ $p130^{cas}$ and DOCK1/DOCK180, both LIF-regulated proteins, are associated with focal adhesions [81, 82].

Integrins and the Extracellular Matrix Proteins Laminin, Fibronectin, Osteopontin, and Muc1

Integrin receptors are made up of alpha and beta subunits, and signaling through this complex is implicated in mediating cell-cell interactions during embryo implantation [83, 84]. This pathway was upregulated at 3 and 6 h. The alpha integrin subunits affected by LIF included integrins A3 (*Itga3*), A5 (*Itga5*), and A6 (*Itga6*), while ITGB5 was the beta integrin that changed. Other responsive genes associated with the integrin-signaling pathway included: dedicator of cytokinesis 1 (*Dock1*), Wiskott-Aldrich syndrome-like (*Wasl*), ras homolog family member B (*Rhob*), ras homolog family member D

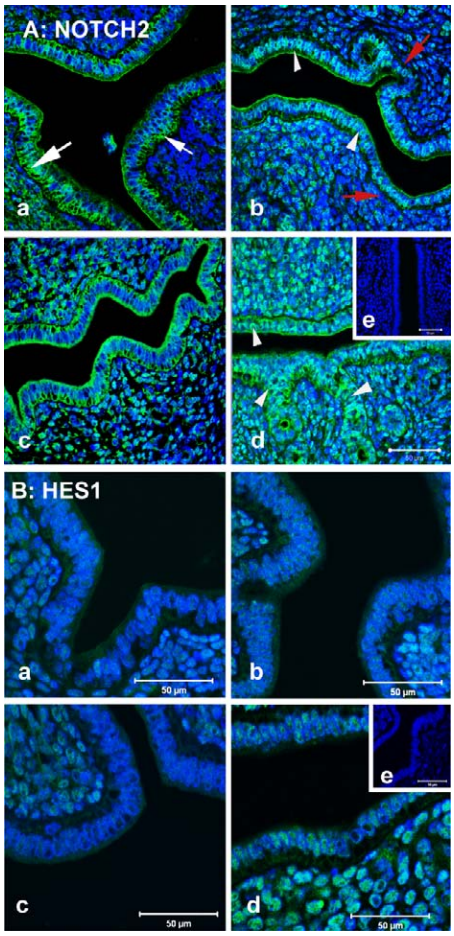

FIG. 7. Alterations in the Notch 2 signaling pathway. **A**) The intracellular domain (ICD) of NOTCH2 (green) localizes to the LE membranes at 1 h and then increases in expression at 3 and 6 h. NOTCH2 ICD then localizes to the nucleus at 6 h (**a**: 0 h; **b**: 1 h; **c**: 3 h; **d**: 6 h; **e**: negative control). White arrows indicate localization of NOTCH2 ICD at the LE membrane; white arrowheads indicate expression in nucleus while red arrows indicate loss of expression at the cell membrane. Bar = 50 μm. **B**) The notch-regulated transcription factor HES1 (green) nuclear localization increases in the LE and stroma by 6 h (**a**: 0 h; **b**: 1 h; **c**: 3 h; **d**: 6 h; **e**: negative control). Bar = 50 μm.

(*Rhod*), and v-ral simian leukemia viral oncogene homolog A (ras related) (*Rala*). We confirmed the alteration in expression of *Itga3* by qPCR analysis. The mRNA for this integrin peaked by 3 h and then declined (Supplemental Fig. S12E).

By immunofluorescence analysis, ITGA3 localized to the apical, basal, and lateral membranes of the LE. By 1 h, expression had declined and by 6 h was restricted to the basal and a lesser extent apical membranes (Fig. 6B). The decrease in ITGA3 was confirmed by Western blot analysis at 3 and 6 h (Supplemental Fig. S12Fa–Fc). The three alpha subunits specifically interact with β1, although α6 can interact with the β4 integrin. Although β1 localized to the basal membrane of the LE, its expression was unaltered by LIF (data not shown). The only subunit that was LIF regulated in the microarray was β5, which undergoes a basal to apical membrane transition in the rat uterine LE at the time of embryo attachment [85]. Whether this integrin subunit forms a unique interaction with the alpha subunits in the untreated LE remains to be determined.

The transcript levels of the two other genes, *Dock1* and *Wasl*, transiently increased by 3 h and then fell by 6 h (Supplemental Fig. S12, G and H). The expression of three major components of the extracellular matrix, laminin, (Laminin C [y] 1), fibronectin (Fn), and osteopontin (*Spp1*)—all Arg-Gly-Asp peptide-containing proteins that bind integrins—was also analyzed. Prior to LIF treatment, the three proteins showed strong expression in the LE with laminin and osteopontin localizing to the apical and basal LE membranes. Fn predominantly localized to the LE cytoplasm, and in contrast to the other two proteins, Fn expression in the LE declined (Fig. 6C). Following LIF treatment, laminin C1 levels in the LE declined but then transiently increased in the sub-LE stroma at 3 h (Fig. 6D). Osteopontin localization to the LE membranes persisted throughout the 6 h period with a marked peak in expression at 3 h (Fig. 6E).

Another extracellular matrix protein that has been extensively investigated regarding its role in regulating implantation is the mucin, *Muc1* [86]. MUC1 expression in the LE is repressed by P4 and is weakly expressed by D4 in the LE of the mouse and rat. In the LIF-treated mice, *Muc1* transcripts and protein levels were low at 0 and 1 h (Fig. 6, Fa and Fb, and Supplemental Fig. S12I) and by 3 h increased MUC1 localized to the apical LE (Fig. 6, Fc and Fd, and Supplemental Fig. S12I). The significance of these changes in SPP1 expression remains to be seen because *Spp1*- and *Muc1*-null mice are fertile as are mice doubly deficient for both *Spp1* and vitronectin [87, 88].

FGF Pathway

Another prominent pathway that was induced was that of FGFs. FGFs have a multitude of regulatory functions in cell proliferation, angiogenesis, wound healing, and development of various tissue/organ systems. Genes whose expression altered following LIF treatment included FGF 1 (*Fgf1*), FGF receptor 2 (*Fgfr2*), Grb2-associated binding protein 1 (*Gab1*), phosphatidylinositol-4,5-bisphosphate 3-kinase, catalytic subunit gamma (*Pik3cg*), heme oxygenase (decycling) 1 (*Hmox1*), and FGFR-like 1 (*Fgfrl1*). FGFs, in particular FGFs 1, 9, 10, 18, and 21, were previously identified in the stroma where they influence LE cell proliferation [46]. Loss of the transcription factors MSX1/2 or HAND2 in the stroma, enhances FGF expression, either by the MSX-regulated WNT pathway and/or HAND2 driven by P4, blocking stromal FGF expression [89]. Stromal FGFs act via their FGFRs in the LE to stimulate the ERK1/2 kinase pathway in both the LE and GE. Consequently, cell proliferation is maintained, with the uterus failing to attain a receptive state [46, 89]. We observed exclusive expression of FGFR2 in the LE, as previously reported (Supplemental Fig. S13C). Its expression, as well as that of its ligand FGF1, declined following LIF treatment (Supplemental Fig. S13A–D). GAB1, a protein phosphorylated by FGF signaling and required to activate PI3K-AKT pathway [90], also fell (Supplemental Fig. S13E). The reduction in FGF signaling during embryo attachment indicates that LIF contributes to the inhibition of this pathway, paralleling the inhibition of the IGF1 pathway.

Notch2 Pathway

Array analysis revealed an increase in *Notch1* expression by 1 h together with increased expression of the Notch-regulated transcription factors HEY2 and HES1. NOTCH1 is implicated at inducing stromal cell decidualization in the mouse uterus [36]; however, we did not detect any changes in expression *Notch1* either by qPCR or by immunofluorescence. Because NOTCH2, another Notch receptor, is expressed in human LE

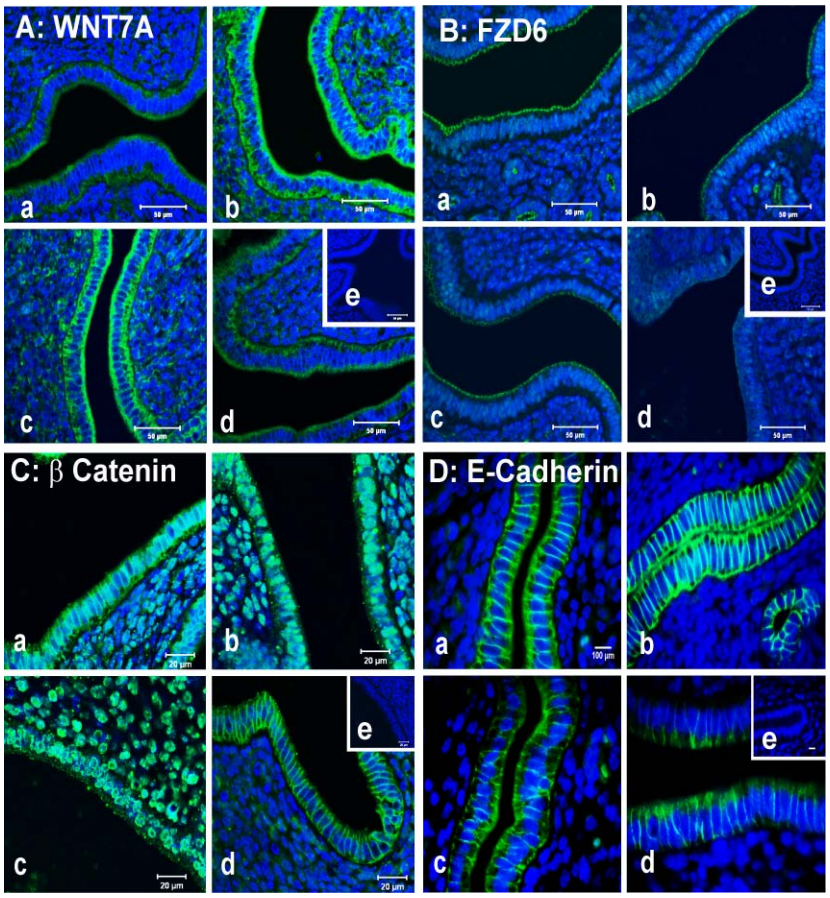

FIG. 8. LIF activates the canonical Wnt pathway. **A**) WNT7A (green) protein increases in the LE at 1 and 3 h and then declines at 6 h. Bar = 50 μm. **B**) FZD6 (green) protein decreases at the apical LE membranes. Bar = 50 μm. **C**) The transcriptionally active dephosphorylated form of β-catenin (in green) shows increased nuclear localization in the LE and stroma 3 and 6 h. Bar = 20 μm. Subpanels indicate expression changes (**a**: 0 h; **b**: 1 h; **c**: 3 h; **d**: 6 h; **e**: negative control). **D**) E-Cadherin (green) expression decreases at the basal membrane of the LE at 6 h. Bar = 100 μm.

[91], we analyzed its expression by qPCR and found *Notch2* transcript levels fell following LIF treatment (Supplemental Fig. S14A). At the protein level, the functional intracellular domain (ICD) of NOTCH2 localized to the apical and basal membranes and cytoplasm by 3 h (Fig. 7Ac), and by 6 h, the ICD was detected in the LE nuclei (Fig. 7Ad). Total protein levels of the Notch2 ICD (cNotch2) had risen by 6 h, (Supplemental Fig. S14B). In parallel, stromal levels of NOTCH2 also increased (Fig. 7Ad).

The only Notch ligand showing a change in expression was Jagged 1 (*Jag1*). Its transcript and protein levels increased at 3 and 6 h (data not shown). Other genes altered in this pathway include *Deltex4, Numb,* and radical fringe (*Rfng*). Notch signaling results in the downstream activation of the hairy and enhancer of split-1 (HES) and hairy/enhancer-of-split related with YRPW motif (HEY) group of transcription factors [92]. We observed increased HES1, but not HEY1 expression, with transcripts and nuclear levels of HES1 increasing in the LE by 6 h (Fig. 7B and Supplemental Fig. S14, C and D). HES1 stromal expression also increased (Fig. 7Bd). Whether such localization in the stroma depends on signaling from the LE remains to be determined.

Canonical Wnt/β Catenin Signaling

The canonical Wnt/β-catenin pathway has been implicated in regulating uterine cell proliferation, blastocyst invasion, and decidualization [93]. Overall, LIF treatment transiently enhanced expression of many genes in this pathway between 1 and 6 h. The only canonical ligand identified was WNT7A. Transcripts of *Wnt7a* increased over the first 3 h and then declined (Supplemental Fig. S15A). WNT7A expression in the LE peaked at 3 h with some expression in the stroma (Fig. 8Ac). Transcript levels of the Wnt receptor, Frizzled homolog 6 (Fzd6), fell over the 6 h (Supplemental Fig. S15B), with reduced protein levels apparent only by 6 h (Fig. 8B and Supplemental Fig. S15, B and C). Other pathway genes identified were *Sry* (sex-determining region Y)-boxes 7 (*Sox7, 9,* and 17), transducinlike enhancer of split 3 (*Esp1*) homolog, Drosophila) (*Tle3*), secreted frizzled-related protein 1 (*Sfrp1*), and gap junction protein, alpha 1, 43kDa (*Gja1*). We observed a significant increase in *Lgr5*, a cofactor for WNT receptors and stem cell marker, in the LE at 3 h, although none of its four coreceptors showed altered expression (data not shown). Beta-catenin, the major cofactor for the TCF/LEF transcription factors, showed reduced transcript levels following treatment (Supplemental Fig. S15F); however, total protein levels remained unaltered (data not shown). Nuclear localization of the transcriptionally active form of β-catenin was detected in the LE and stroma within 1 h of LIF administration (Fig. 8, Cb and Cc). By 6 h, nuclear localization had declined, and β-catenin reverted back to the cell membrane in LE and was reduced in the stroma (Fig. 8Cd). Wnt signaling is thought to be dependent on the presence of implanting blastocysts [94], but we predict that an active Wnt/β-catenin pathway, independent of embryos, is induced in the LE before

implantation because we noted strong nuclear localization of β-catenin in the LE at 1 h (Fig. 8C).

The adherens junction protein E-Cadherin, which interacts with β-catenin, showed a decline in overall transcript and protein levels by 6 h (Fig. 8D and Supplemental Fig. S15, D and E). Immunolocalization revealed E-Cadherin was expressed exclusively in the LE apical, basal, and lateral membranes. By 6 h, the basal localization of E-cadherin expression had declined, whereas apical expression persisted (Fig. 8Cd). Such apical localization persists to D5 of pregnancy (data not shown).

Tgfβ Superfamily Pathway

The transforming growth factor beta (*TGFβ*) signaling pathway is upregulated at 3 and 6 h. In this pathway, the genes showing changes in expression were the activin receptors type 1 (*Acvr1*), type 2B (*Acvr2b*), *TGF-β* receptor 1 (*Tbfbr1*), and the *TGF-β* receptor 2 (*Tgfbr2*). The other genes induced were *TGF-β*2 (*Tgfb2*), the TGFβ-induced factor homeobox 1 (*Tgif1*), related RAS viral (r-ras) oncogene homolog 2 (*Rras2*). *Bmp2*, which mediates stromal decidualization, was not detected. We validated the transcript expression of *Acvr1, Tgfb2,* and *Rras2* by qPCR. *Tgf*β*2* transcript levels increased over 6 hours (Supplemental Fig. S16A), whereas expression of both *Acvr1* and *Rras2* maximized by 3 h but declined by 6 h (Supplemental Fig. S16, B and C).

ACVR1 protein was expressed predominantly in the LE, GE, and subepithelial stroma at 0 h (Fig. 9Aa). ACVR1 expression then transiently declined in the stroma, GE, and LE (Fig. 9b), but by 3 and 6 h, expression had increased in the LE and slightly in the subepithelial stroma (Fig. 9, Ac and Ad). Similarly TGFβR1 was maximally expressed in the LE, GE, and subepithelial stroma at 0 h (Fig. 9Ba), and then also transiently declined in the LE at 1 h. TGFβR1 in the subepithelial stroma was not detected (Fig. 9Bb). However, by 3 and 6 h, TGFβR1 expression had increased in the LE, with some increase in the subepithelial stroma (Fig. 9, Bc and Bd).

TGFβ pathway mediates transcription by phosphorylation and nuclear translocation of SMAD2/SMAD3 proteins. Although the array analysis did not show any changes in the expression of either of these proteins, alterations in SMAD3 phosphorylation and localization were detected. At 0 h, pSMAD3 appeared to localize to the apical submembranous cytoplasm and remained unchanged throughout the subsequent 6 h (Fig. 9Ca). However within 1 h, nuclear localization of pSMAD3 was observed throughout the LE and had also increased in the stroma (Fig. 9Cb). By 6 h, pSMAD3 expression had reverted back to the levels and distribution seen at 0 h (Fig. 9Cd). Stromal expression however declined by 3 h and was absent by 6 h (Fig. 9, Cc and Cd). Array analysis indicated that SMAD5 was the only SMAD protein increased by 3 h. Analysis revealed a fall in pSMAD5 nuclear localization in the LE at 3 h, followed by an increase at 6 h (Fig. 9, Dc and Dd). Cytoplasmic expression increased at 3 h but subsequently declined by 6 h (Fig. 9, Dc and Dd). In the stroma, increased expression of nuclear pSMAD5 was noted at 3 and 6 h (Fig. 9, Dc and Dd).

DISCUSSION

Uterine receptivity in mice is regulated by the secreted cytokine LIF binding to LIFRs on the LE. A single intraperitoneal injection of 10 μg LIF (which has an in vivo half-life of 6–8 min [95]) initiates phosphorylation of the transcription factor STAT3 that then translocates to the LE nuclei within 1 h. The GE also expresses the LIF receptor complex, as well as STAT3, although STAT3 does not appear to translocate to the nucleus, possibly because the PGR is not expressed in the GE, since the PGR can act as a transcriptional cofactor with pSTAT3 [96]. In mice lacking LIF; in mutations in the LIFr/GP130 receptor complex [97]; or where the LIFRβ or STAT3 was specifically deleted in the LE [96, 98] (Cheng JG, Rosario G, Cohen TV, Hu J, Stewart CL, unpublished data), the JAK-STAT pathway is not activated. All of these mutated mice exhibit implantation failure as do mice treated with small molecule inhibitors of the JAK-STAT pathway [99–101]. Furthermore, monkeys treated with monoclonal antibodies to LIF similarly exhibited pregnancy failure [102]. In contrast, blastocysts lacking either GP130 and/or the LIFR can implant and undergo a few days of postimplantation development, indicating that a functional LIF/GP130 receptor is not required by the blastocyst at implantation [103]. Together these results demonstrate that LIF primarily act on the LE, and in mice its expression is only required once to initiate implantation, rather than biphasically as previously suggested [14, 104, 105].

Here we employed microarray screening coupled with informatics analysis to identify genes differentially induced in the prereceptive LE in response to LIF. Our goal was to characterize the molecular signature of the switch from a prereceptive to receptive LE. By using *ovxd*, hormonally primed mice this controlled regimen is nevertheless sufficient to support blastocyst implantation and subsequent normal postimplantation development [106, 107]. By using this system, we were able to precisely record the dynamic and transient changes in gene and corresponding protein expression, which would likely have been missed using naturally mated animals.

Only three studies on LE-specific changes in the mouse have been reported [25, 35, 108], and of these, two described changes induced within 3 h of injecting of nidatory E_2, following priming by E_2 and P4 in ovxd mice [35, 108]. This time point was probably comparable to the changes within 2 h after LIF injection because LIF is induced within 1 h of E_2 injection [7]. We extended this approach by identifying genes regulated by LIF at four time points over 6 h with regard to both overall gene expression and to characterizing the dynamic changes in expression and localization of the proteins encoded by some of these genes.

Initially, we focused on changes induced within the first hour after LIF treatment. This was because we felt that such changes would likely include those directly induced by LIF/STAT3 and exclude secondary changes resulting from the induction of the 40-plus transcription factors induced within 1 h after LIF. Our analysis identified 54 annotated genes whose expression declined. These were grouped into two GO classes, specifically those involved in cytoskeletal organization—including the cytokeratins (Krt 5, 14, 15, and 17) and proteins organizing the actin cytoskeleton (*Arc*, *Cfl1*)—and those required for tight junction and hemidesmosome function, including claudin and collagen 17 (*Cldn5*, *Col1a1*). The other group of genes that declined was those involved in maintaining heterochromatin, and included chromobox 8 homolog (*Cbx8*), the histone methylase *Suv420h2*, as well as the histone clusters Hist1h4k and Hist4h4. In addition, the transcription factor *Mig-6,* which suppresses E_2-driven uterine proliferation [109], *Tob1,* which inhibits cell proliferation, and *Cited2* (Cbp/p300-interacting transactivator), a P4-regulated gene that stimulates the hypoxia inducible transcription factor *Hif-1α*, were also reduced. Intriguingly, two other genes with reduced expression were *Per1* and *Rgs16,* both of which are involved in regulating

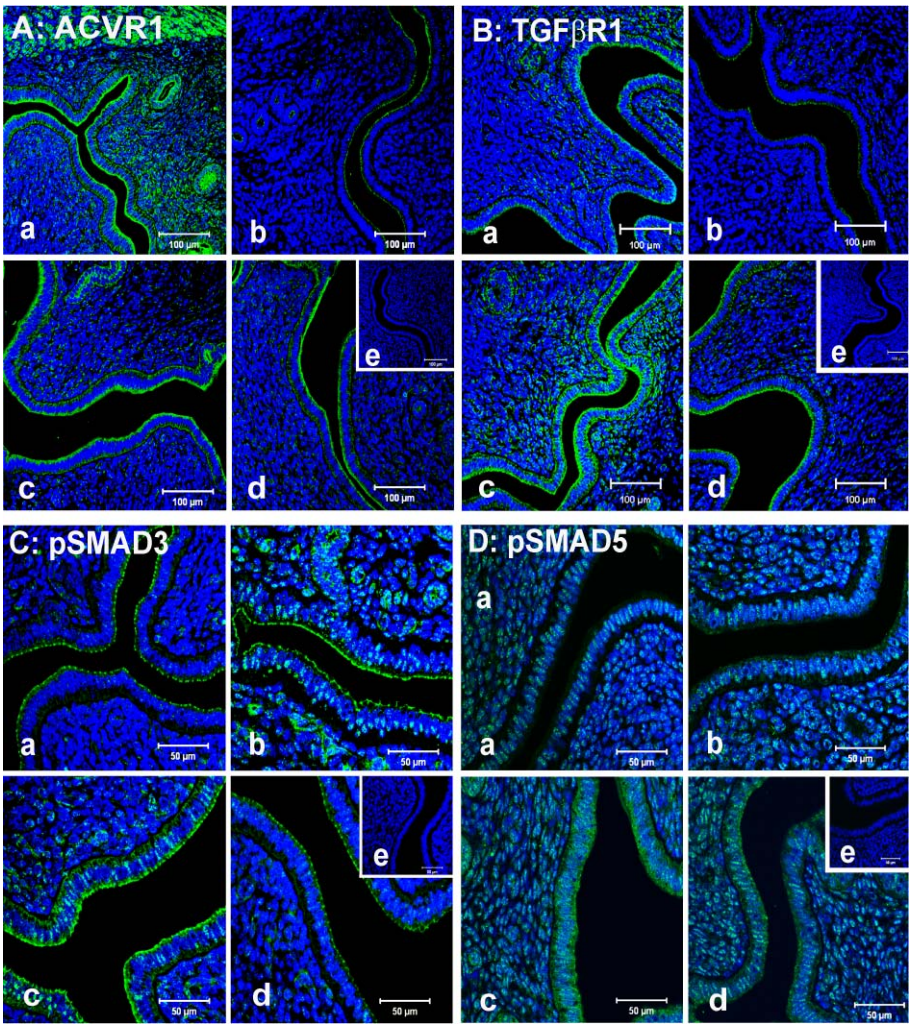

FIG. 9. The *TGFβ* superfamily pathways are regulated by LIF. **A**) Expression of the receptor ACVR1 protein (in green) predominantly in the LE and marginally in the subepithelial stroma at 0 h. ACVR1 expression in the stroma and LE transiently declines by 1 h, but by 3 h, ACVR1 returns to the LE and slightly in the subepithelial stroma. Subpanels indicate expression (**a**: 0 h; **b**: 1 h; **c**: 3 h; **d**: 6 h; **e**: negative control). Bar = 100 μm. **B**) TGFβR1 (in green) expression transiently declines in the LE and subepithelial stroma by 1 h. Expression of TGFβR1 is restored to the LE and subepithelial stroma by 3 h. Subpanels indicate expression changes (**a**: 0 h; **b**: 1 h; **c**: 3 h; **d**: 6 h; **e**: negative control). Bar = 100 μm. **C**) Nuclear translocation of pSMAD3 (green) is induced by LIF at 1 h in LE and stroma and then falls. Subpanels indicate expression changes (**a**: 0 h; **b**: 1 h; **c**: 3 h; **d**: 6 h; **e**: negative control). Bar = 50 μm. **D**) Nuclear translocation of pSMAD5 (green) is induced at 3 and 6 h in the stroma but levels fall in the LE at the same time points. Subpanels indicate expression changes (**a**: 0 h; **b**: 1 h; **c**: 3 h; **d**: 6 h; **e**: negative control). Bar = 50 μm.

circadian rhythms, with *Per1* being potentially transcriptionally regulated by the PGR in the uterus [53]. Together these findings suggest that loss of the non- or prereceptive state requires a reduction in cytoskeletal/cell adhesion integrity coupled with a reduction in heterochromatin.

In contrast to the relatively low number of genes whose expression declines, some 256 genes were induced within 1 h of LIF treatment in the LE. This number was similar to that induced in the LE by nidatory E_2 (222) [35]. However, of these, only 36 were common to both lists (Supplemental Table S7) suggesting that these 36 genes, following nidatory E_2, may be directly regulated by LIF. In the LIF-stimulated mice, ESR does not show strong LE expression until 3 h after LIF injection, implying that all the transcriptional changes observed in the LE within the first hour are induced independent of the ESR. In contrast, the PGR is expressed at 0 h in LE nuclei although, intriguingly, within 1 h it transiently disappears from the nuclei, with strong nuclear localization being restored after 3 h. The dynamics of these changes suggest that the PGR functions, perhaps transiently, with STAT3 in regulating gene expression between 0 and 1 h after LIF treatment, in support of a previous study [96]. The absence of nuclear PGR at 1 h also correlates with the transient increase and nuclear localization of Cyclin D1, which is regulated by the P4 [38] (Fig. 3Cb) and the loss of TGFβR1 and ACVR1 protein in the LE at the same time (Fig. 9Bb), indicating that the changes associated with the onset of uterine receptivity are rapid and dynamic.

By 3 h post-LIF treatment, the number of genes exhibiting altered expression levels increased to over 4000. Such a large number of changes is likely related to the induction of over 40 transcription factors (some previously identified) within the first hour after LIF, including *Sox7, 9,* and *17, Hoxd10* and *b4, Klf6* and *9*, *Hes1, Hey2, Irf1,* and *Stat3* (Supplemental Table S6). Some of the genes induced in the LE, were also induced in the stroma by 3 h, indicating that LIF indirectly influences stromal gene expression, perhaps by initiating the expression of some yet-to-be-identified cytokine/GF in the LE that acts on the stromal cells. Potential candidates included parathyroid hormonelike peptide (*PThrP*), follistatinlike 1, *Ccl7, 2, Cxcl, 1, 10, 14, Ihh, ghrelin, Bdnf,* or *Csf3*.

We identified 25 distinct pathways that were affected by LIF treatment. Our GO analysis of BP functions identified that blood vessel formation/vasculogenesis, inflammation, response to hormone stimulus, transcription, regulation of apoptosis, cell proliferation, the cytoskeleton, and cell adhesion as being the most significantly induced BP clusters. IPA analysis identified many canonical signaling pathways that presumably control these BPs, including the VEGF/HIF-1α, FGF, and NOTCH pathways regulating vasculogenesis; the TOLL-NFkB pathways regulating inflammation, innate immunity, and cell stress/apoptosis; mTOR, IGF1, TGFβ superfamily, and FGF pathways regulating metabolism and cell proliferation; and others, such as the WNT and Ephrin pathways, that potentially regulate cytoskeletal organization/cell adhesion. The identification of these BPs was in broad agreement with many previous studies, with the important addition that we demonstrated that multiple signaling pathways may simultaneously regulate these BPs. Within 3 h of LIF administration, the numbers of genes whose expression changes is maximized. Thereafter the number of affected genes starts to decline, with evidence pointing to the LE/uterus reverting to a nonreceptive state within 6 h.

We have documented the changes that a simple epithelium, the LE, undergoes in switching from a refractory/nonresponsive state to a responsive LE, due to a single cytokine, LIF. This included an extensive immunohistochemical analysis of some of the proteins encoded by these genes; we found that the responses were characterized by relatively rapid changes in the subcellular relocalization and distribution of many of these proteins, revealing the molecular responses to LIF is often fleeting and highly dynamic. Combined, these changes in gene expression result in the activation of many BPs in anticipation of blastocysts implantation. Determining which of these changes is essential for successful embryo implantation using tissue-specific *Cre*-mediated ablation has provided much important information. These procedures however require the time-consuming and expensive breeding of mice. Furthermore, many of the genes used to specifically express the *Cre* recombinase are naturally expressed during uterine development. As a consequence, it is difficult to determine whether any defect arising in implantation/decidualization is due to some developmental defect arising from ablation of the gene, for example, failure to form the endometrial glands being a frequent consequence of using the PR-*cre* line of mice, rather than to an immediate requirement of the gene in the implantation/decidualization process [77, 110–112]. This will necessitate the development of relatively simple and efficient methods to disrupt specific gene expression, which may include small molecule inhibitors, the introduction of antisense RNAs, and/or the efficient ablation of specific genes. Because LIF may also be critical to endometrial receptivity in humans, as well as a wide range of other mammals, with reduced LIF expression being linked to several cases of female infertility, information on LIF-driven gene networks will be beneficial in generating effective treatment strategies for human implantation-related infertility.

ACKNOWLEDGMENT

We thank K. Rogers, for advice on histological procedures, V. Tanavde, for help on microarray analysis, and B. Lane, P. Sampath and R Dunn for antibodies. The Notch 2 intracellular domain monoclonal antibody developed by Dr. S. Artavanis-Tsakonas, Dept. of Cell Biology, Harvard Medical School, Boston, MA, was obtained from the Developmental Studies Hybridoma Bank under the auspices of the NICHD and maintained by The University of Iowa, Dept. of Biology, Iowa City, IA. We also wish to thank Lucy Robinson of Insight Editing London for critical review of the manuscript.

REFERENCES

1. Finn CA, Martin L. The control of implantation. J Reprod Fertil 1974; 39:195–206.
2. Groothuis PG, Dassen HH, Romano A, Punyadeera C. Estrogen and the endometrium: lessons learned from gene expression profiling in rodents and human. Hum Reprod Update 2007; 13:405–417.
3. Psychoyos A. Hormonal control of ovoimplantation. Vitam Horm 1973; 31:201–256.
4. Lim HJ, Wang H. Uterine disorders and pregnancy complications: insights from mouse models. J Clin Invest 2010; 120:1004–1015.
5. Ramathal CY, Bagchi IC, Taylor RN, Bagchi MK. Endometrial decidualization: of mice and men. Semin Reprod Med 2010; 28:17–26.
6. Stewart CL, Kaspar P, Brunet LJ, Bhatt H, Gadi I, Kontgen F, Abbondanzo SJ. Blastocyst implantation depends on maternal expression of leukaemia inhibitory factor [see comments]. Nature 1992; 359:76–79.
7. Chen JR, Cheng JG, Shatzer T, Sewell L, Hernandez L, Stewart CL. Leukemia inhibitory factor can substitute for nidatory estrogen and is essential to inducing a receptive uterus for implantation but is not essential for subsequent embryogenesis. Endocrinology 2000; 141: 4365–4372.
8. Hu W, Feng Z, Teresky AK, Levine AJ. p53 regulates maternal reproduction through LIF. Nature 2007; 450:721–724.
9. Bhatt H, Brunet LJ, Stewart CL. Uterine expression of leukemia inhibitory factor coincides with the onset of blastocyst implantation. Proc Natl Acad Sci U S A 1991; 88:11408–11412.
10. Shen MM, Leder P. Leukemia inhibitory factor is expressed by the preimplantation uterus and selectively blocks primitive ectoderm formation in vitro. Proc Natl Acad Sci U S A 1992; 89:8240–8244.
11. Cullinan EB, Abbondanzo SJ, Anderson PS, Pollard JW, Lessey BA, Stewart CL. Leukemia inhibitory factor (LIF) and LIF receptor expression in human endometrium suggests a potential autocrine/paracrine function in regulating embryo implantation. Proc Natl Acad Sci U S A 1996; 93:3115–3120.
12. Song JH, Houde A, Murphy BD. Cloning of leukemia inhibitory factor (LIF) and its expression in the uterus during embryonic diapause and implantation in the mink (*Mustela vison*). Mol Reprod Dev 1998; 51: 13–21.
13. Cheng JG, Chen JR, Hernandez L, Alvord WG, Stewart CL. Dual control of LIF expression and LIF receptor function regulate Stat3 activation at the onset of uterine receptivity and embryo implantation. Proc Natl Acad Sci U S A 2001; 98:8680–8685.
14. Song H, Lim H. Evidence for heterodimeric association of leukemia inhibitory factor (LIF) receptor and gp130 in the mouse uterus for LIF signaling during blastocyst implantation. Reproduction 2006; 131: 341–349.
15. Auernhammer CJ, Melmed S. Leukemia-inhibitory factor-neuroimmune modulator of endocrine function. Endocr Rev 2000; 21:313–345.
16. Sherwin JR, Smith SK, Wilson A, Sharkey AM. Soluble gp130 is up-regulated in the implantation window and shows altered secretion in patients with primary unexplained infertility. J Clin Endocrinol Metab 2002; 87:3953–3960.
17. Takamoto N, Zhao B, Tsai SY, DeMayo FJ. Identification of Indian hedgehog as a progesterone-responsive gene in the murine uterus. Mol Endocrinol 2002; 16:2338–2348.
18. Rodriguez CI, Cheng JG, Liu L, Stewart CL. Cochlin, a secreted von Willebrand factor type a domain-containing factor, is regulated by leukemia inhibitory factor in the uterus at the time of embryo implantation. Endocrinology 2004; 145:1410–1418.
19. Sherwin JR, Freeman TC, Stephens RJ, Kimber S, Smith AG, Chambers I, Smith SK, Sharkey AM. Identification of genes regulated by leukemia-inhibitory factor in the mouse uterus at the time of implantation. Mol Endocrinol 2004; 18:2185–2195.
20. Catalano RD, Johnson MH, Campbell EA, Charnock-Jones DS, Smith SK, Sharkey AM. Inhibition of Stat3 activation in the endometrium prevents implantation: a nonsteroidal approach to contraception. Proc Natl Acad Sci U S A 2005; 102:8585–8590.
21. Wakitani S, Hondo E, Phichitraslip T, Stewart CL, Kiso Y. Upregulation of Indian hedgehog gene in the uterine epithelium by leukemia inhibitory factor during mouse implantation. J Reprod Dev 2008; 54:113–116.
22. Daikoku T, Song H, Guo Y, Riesewijk A, Mosselman S, Das SK, Dey SK. Uterine Msx-1 and Wnt4 signaling becomes aberrant in mice with the loss of leukemia inhibitory factor or Hoxa-10: evidence for a novel cytokine-homeobox-Wnt signaling in implantation. Mol Endocrinol 2004; 18:1238–1250.

23. Bany BM, Schultz GA. Increased expression of a novel heat shock protein transcript in the mouse uterus during decidualization and in response to progesterone. Biol Reprod 2001; 64:284–292.
24. Baran N, Kelly PA, Binart N. Characterization of a prolactin-regulated gene in reproductive tissues using the prolactin receptor knockout mouse model. Biol Reprod 2002; 66:1210–1218.
25. Campbell EA, O'Hara L, Catalano RD, Sharkey AM, Freeman TC, Johnson MH. Temporal expression profiling of the uterine luminal epithelium of the pseudo-pregnant mouse suggests receptivity to the fertilized egg is associated with complex transcriptional changes. Hum Reprod 2006; 21:2495–2513.
26. Chen Y, Ni H, Ma XH, Hu SJ, Luan LM, Ren G, Zhao YC, Li SJ, Diao HL, Xu X, Zhao ZA, Yang ZM. Global analysis of differential luminal epithelial gene expression at mouse implantation sites. J Mol Endocrinol 2006; 37:147–161.
27. Franco HL, Lee KY, Broaddus RR, White LD, Lanske B, Lydon JP, Jeong JW, DeMayo FJ. Ablation of Indian hedgehog in the murine uterus results in decreased cell cycle progression, aberrant epidermal growth factor signaling, and increased estrogen signaling. Biol Reprod 2010; 82: 783–790.
28. Huang ZP, Ni H, Yang ZM, Wang J, Tso JK, Shen QX. Expression of regulator of G-protein signalling protein 2 (RGS2) in the mouse uterus at implantation sites. Reproduction 2003; 126:309–316.
29. Kao LC, Tulac S, Lobo S, Imani B, Yang JP, Germeyer A, Osteen K, Taylor RN, Lessey BA, Giudice LC. Global gene profiling in human endometrium during the window of implantation. Endocrinology 2002; 143:2119–2138.
30. Larose M, St-Amand J, Yoshioka M, Belleau P, Morissette J, Labrie C, Raymond V, Labrie F. Transcriptome of mouse uterus by serial analysis of gene expression (SAGE): comparison with skeletal muscle. Mol Reprod Dev 2004; 68:142–148.
31. Ma XH, Hu SJ, Ni H, Zhao YC, Tian Z, Liu JL, Ren G, Liang XH, Yu H, Wan P, Yang ZM. Serial analysis of gene expression in mouse uterus at the implantation site. J Biol Chem 2006; 281:9351–9360.
32. Matsumoto Y, Handa S, Taki T. gp49B1, an inhibitory signaling receptor gene of hematopoietic cells, is induced by leukemia inhibitory factor in the uterine endometrium just before implantation. Dev Growth Differ 1997; 39:591–597.
33. Nie GY, Li Y, Batten L, Griffiths B, Wang J, Findlay JK, Salamonsen LA. Uterine expression of alternatively spliced mRNAs of mouse splicing factor SC35 during early pregnancy. Mol Hum Reprod 2000; 6: 1131–1139.
34. Nie GY, Li Y, Hampton AL, Salamonsen LA, Clements JA, Findlay JK. Identification of monoclonal nonspecific suppressor factor beta (mNSFbeta) as one of the genes differentially expressed at implantation sites compared to interimplantation sites in the mouse uterus. Mol Reprod Dev 2000; 55:351–363.
35. Pan H, Zhu L, Deng Y, Pollard JW. Microarray analysis of uterine epithelial gene expression during the implantation window in the mouse. Endocrinology 2006; 147:4904–4916.
36. Afshar Y, Jeong JW, Roqueiro D, DeMayo F, Lydon J, Radtke F, Radnor R, Miele L, Fazleabas A. Notch1 mediates uterine stromal differentiation and is critical for complete decidualization in the mouse. FASEB J 2012; 26:282–294.
37. Lejeune B, Van Hoeck J, Leroy F. Transmitter role of the luminal uterine epithelium in the induction of decidualization in rats. J Reprod Fertil 1981; 61:235–240.
38. Tong W, Pollard JW. Progesterone inhibits estrogen-induced cyclin D1 and cdk4 nuclear translocation, cyclin E- and cyclin A-cdk2 kinase activation, and cell proliferation in uterine epithelial cells in mice. Mol Cell Biol 1999; 19:2251–2264.
39. Bigsby RM, Cooke PS, Cunha GR. A simple efficient method for separating murine uterine epithelial and mesenchymal cells. Am J Physiol 1986; 251:E630–E636.
40. Huang da W Sherman BT , Lempicki RA. Bioinformatics enrichment tools: paths toward the comprehensive functional analysis of large gene lists. Nucleic Acids Res 2009; 37:1–13.
41. Schnell SA, Staines WA, Wessendorf MW. Reduction of lipofuscin-like autofluorescence in fluorescently labeled tissue. J Histochem Cytochem 1999; 47:719–730.
42. Fagg B, Martin L, Rogers L, Clark B, Quarmby VE. A simple method for removing the luminal epithelium of the mouse uterus for biochemical studies. J Reprod Fertil 1979; 57:335–339.
43. Tan J, Paria BC, Dey SK, Das SK. Differential uterine expression of estrogen and progesterone receptors correlates with uterine preparation for implantation and decidualization in the mouse. Endocrinology 1999; 140:5310–5321.
44. Hewitt SC, Li Y, Li L, Korach KS. Estrogen-mediated regulation of Igf1 transcription and uterine growth involves direct binding of estrogen receptor alpha to estrogen-responsive elements. J Biol Chem 2010; 285: 2676–2685.
45. Daikoku T, Cha J, Sun X, Tranguch S, Xie H, Fujita T, Hirota Y, Lydon J, DeMayo F, Maxson R, Dey SK. Conditional deletion of Msx homeobox genes in the uterus inhibits blastocyst implantation by altering uterine receptivity. Dev Cell 2011; 21:1014–1025.
46. Nallasamy S, Li Q, Bagchi MK, Bagchi IC. Msx homeobox genes critically regulate embryo implantation by controlling paracrine signaling between uterine stroma and epithelium. PLoS Genet 2012; 8:e1002500.
47. Franco HL, Rubel CA, Large MJ, Wetendorf M, Fernandez-Valdivia R, Jeong JW, Spencer TE, Behringer RR, Lydon JP, Demayo FJ. Epithelial progesterone receptor exhibits pleiotropic roles in uterine development and function. FASEB J 2012; 26:1218–1227.
48. Fouladi-Nashta AA, Jones CJ, Nijjar N, Mohamet L, Smith A, Chambers I, Kimber SJ. Characterization of the uterine phenotype during the peri-implantation period for LIF-null, MF1 strain mice. Dev Biol 2005; 281: 1–21.
49. Kimber SJ. Leukaemia inhibitory factor in implantation and uterine biology. Reproduction 2005; 130:131–145.
50. Chakraborty I, Das SK, Wang J, Dey SK. Developmental expression of the cyclo-oxygenase-1 and cyclo-oxygenase-2 genes in the peri-implantation mouse uterus and their differential regulation by the blastocyst and ovarian steroids. J Mol Endocrinol 1996; 16:107–122.
51. Huang HL, Chu ST, Chen YH. Ovarian steroids regulate 24p3 expression in mouse uterus during the natural estrous cycle and the preimplantation period. J Endocrinol 1999; 162:11–19.
52. Korgun ET, Cayli S, Asar M, Demir R. Distribution of laminin, vimentin and desmin in the rat uterus during initial stages of implantation. J Mol Histol 2007; 38:253–260.
53. Rubel CA, Lanz RB, Kommagani R, Franco HL, Lydon JP, DeMayo FJ. Research resource: genome-wide profiling of progesterone receptor binding in the mouse uterus. Mol Endocrinol 2012; 26:1428–1442.
54. Winuthayanon W, Hewitt SC, Orvis GD, Behringer RR, Korach KS. Uterine epithelial estrogen receptor alpha is dispensable for proliferation but essential for complete biological and biochemical responses. Proc Natl Acad Sci U S A 2010; 107:19272–19277.
55. Zhu L, Pollard JW. Estradiol-17beta regulates mouse uterine epithelial cell proliferation through insulin-like growth factor 1 signaling. Proc Natl Acad Sci U S A 2007; 104:15847–15851.
56. Warsito D, Sjostrom S, Andersson S, Larsson O, Sehat B. Nuclear IGF1R is a transcriptional co-activator of LEF1/TCF. EMBO Rep 2012; 13:244–250.
57. Tong W, Pollard JW. Genetic evidence for the interactions of cyclin D1 and p27(Kip1) in mice. Mol Cell Biol 2001; 21:1319–1328.
58. Aleksic T, Chitnis MM, Perestenko OV, Gao S, Thomas PH, Turner GD, Protheroe AS, Howarth M, Macaulay VM. Type 1 insulin-like growth factor receptor translocates to the nucleus of human tumor cells. Cancer Res 2010; 70:6412–6419.
59. Sehat B, Tofigh A, Lin Y, Trocme E, Liljedahl U, Lagergren J, Larsson O. SUMOylation mediates the nuclear translocation and signaling of the IGF-1 receptor. Sci Signal 2010; 3. ra10.
60. Rabbani ML, Rogers PA. Role of vascular endothelial growth factor in endometrial vascular events before implantation in rats. Reproduction 2001; 122:85–90.
61. Girling JE, Rogers PA. Regulation of endometrial vascular remodelling: role of the vascular endothelial growth factor family and the angiopoietin-TIE signalling system. Reproduction 2009; 138:883–893.
62. Feng Y, Venema VJ, Venema RC, Tsai N, Caldwell RB. VEGF induces nuclear translocation of Flk-1/KDR, endothelial nitric oxide synthase, and caveolin-1 in vascular endothelial cells. Biochem Biophys Res Commun 1999; 256:192–197.
63. Kazi AA, Molitoris KH, Koos RD. Estrogen rapidly activates the PI3K/AKT pathway and hypoxia-inducible factor 1 and induces vascular endothelial growth factor A expression in luminal epithelial cells of the rat uterus. Biol Reprod 2009; 81:378–387.
64. Kubota Y, Hirashima M, Kishi K, Stewart CL, Suda T. Leukemia inhibitory factor regulates microvessel density by modulating oxygen-dependent VEGF expression in mice. J Clin Invest 2008; 118: 2393–2403.
65. Kawai T, Takeuchi O, Fujita T, Inoue J, Muhlradt PF, Sato S, Hoshino K, Akira S. Lipopolysaccharide stimulates the MyD88-independent pathway

and results in activation of IFN-regulatory factor 3 and the expression of a subset of lipopolysaccharide-inducible genes. J Immunol 2001; 167: 5887–5894.
66. Fazeli A, Bruce C, Anumba DO. Characterization of Toll-like receptors in the female reproductive tract in humans. Hum Reprod 2005; 20: 1372–1378.
67. Py BF, Gonzalez SF, Long K, Kim MS, Kim YA, Zhu H, Yao J, Degauque N, Villet R, Ymele-Leki P, Gadjeva M, Pier GB, et al. Cochlin produced by follicular dendritic cells promotes antibacterial innate immunity. Immunity 2013; 38:1063–1072.
68. Abbondanzo SJ, Cullinan EB, McIntyre K, Labow MA, Stewart CL. Reproduction in mice lacking a functional type 1 IL-1 receptor. Endocrinology 1996; 137:3598–3601.
69. Haziot A, Ferrero E, Kontgen F, Hijiya N, Yamamoto S, Silver J, Stewart CL, Goyert SM. Resistance to endotoxin shock and reduced dissemination of gram-negative bacteria in CD14-deficient mice. Immunity 1996; 4:407–414.
70. Murphy CR. The cytoskeleton of uterine epithelial cells: a new player in uterine receptivity and the plasma membrane transformation. Hum Reprod Update 1995; 1:567–580.
71. Quinn CE, Detmar J, Casper RF. Pinopodes are present in Lif null and Hoxa10 null mice. Fertil Steril 2007; 88:1021–1028.
72. Reardon SN, King ML, MacLean JA II, Mann JL, DeMayo FJ, Lydon JP, Hayashi K. CDH1 is essential for endometrial differentiation, gland development, and adult function in the mouse uterus. Biol Reprod 2012; 86(141):141–110.
73. Jha RK, Titus S, Saxena D, Kumar PG, Laloraya M. Profiling of E-cadherin, beta-catenin and Ca(2+) in embryo-uterine interactions at implantation. FEBS Lett 2006; 580:5653–5660.
74. Pasquale EB. Eph-ephrin bidirectional signaling in physiology and disease. Cell 2008; 133:38–52.
75. Fujii H, Tatsumi K, Kosaka K, Yoshioka S, Fujiwara H, Fujii S. Eph-ephrin A system regulates murine blastocyst attachment and spreading. Dev Dyn 2006; 235:3250–3258.
76. Fujii H, Fujiwara H, Horie A, Sato Y, Konishi I. Ephrin A1 induces intercellular dissociation in Ishikawa cells: possible implication of the Eph-ephrin A system in human embryo implantation. Hum Reprod 2011; 26:299–306.
77. Duffy SL, Coulthard MG, Spanevello MD, Herath NI, Yeadon TM, McCarron JK, Carter JC, Tonks ID, Kay GF, Phillips GE, Boyd AW. Generation and characterization of EphA1 receptor tyrosine kinase reporter knockout mice. Genesis 2008; 46:553–561.
78. Lai KO, Chen Y, Po HM, Lok KC, Gong K, Ip NY. Identification of the Jak/Stat proteins as novel downstream targets of EphA4 signaling in muscle: implications in the regulation of acetylcholinesterase expression. J Biol Chem 2004; 279:13383–13392.
79. Tye H, Kennedy CL, Najdovska M, McLeod L, McCormack W, Hughes N, Dev A, Sievert W, Ooi CH, Ishikawa TO, Oshima H, Bhathal PS, et al. STAT3-driven upregulation of TLR2 promotes gastric tumorigenesis independent of tumor inflammation. Cancer Cell 2012; 22:466–478.
80. Miao H, Burnett E, Kinch M, Simon E, Wang B. Activation of EphA2 kinase suppresses integrin function and causes focal-adhesion-kinase dephosphorylation. Nat Cell Biol 2000; 2:62–69.
81. Carter N, Nakamoto T, Hirai H, Hunter T. EphrinA1-induced cytoskeletal re-organization requires FAK and p130(cas). Nat Cell Biol 2002; 4:565–573.
82. Kiyokawa E, Hashimoto Y, Kurata T, Sugimura H, Matsuda M. Evidence that DOCK180 up-regulates signals from the CrkII-p130(Cas) complex. J Biol Chem 1998; 273:24479–24484.
83. Lessey BA. Adhesion molecules and implantation. J Reprod Immunol 2002; 55:101–112.
84. Singh H, Aplin JD. Adhesion molecules in endometrial epithelium: tissue integrity and embryo implantation. J Anat 2009; 215:3–13.
85. Kaneko Y, Lecce L, Day ML, Murphy CR. beta(1) and beta(3) integrins disassemble from basal focal adhesions and beta(3) integrin is later localised to the apical plasma membrane of rat uterine luminal epithelial cells at the time of implantation.Reprod Fertil Dev 2011; 23:481–495.
86. Surveyor GA, Gendler SJ, Pemberton L, Das SK, Chakraborty I, Julian J, Pimental RA, Wegner CC, Dey SK, Carson DD. Expression and steroid hormonal control of Muc-1 in the mouse uterus. Endocrinology 1995; 136:3639–3647.
87. Liaw L, Birk DE, Ballas CB, Whitsitt JS, Davidson JM, Hogan BL. Altered wound healing in mice lacking a functional osteopontin gene (spp1). J Clin Invest 1998; 101:1468–1478.
88. Spicer AP, Rowse GJ, Lidner TK, Gendler SJ. Delayed mammary tumor progression in Muc-1 null mice. J Biol Chem 1995; 270:30093–30101.
89. Li Q, Kannan A, DeMayo FJ, Lydon JP, Cooke PS, Yamagishi H, Srivastava D, Bagchi MK, Bagchi IC. The antiproliferative action of progesterone in uterine epithelium is mediated by Hand2. Science 2011; 331:912–916.
90. Eswarakumar VP, Lax I, Schlessinger J. Cellular signaling by fibroblast growth factor receptors. Cytokine Growth Factor Rev 2005; 16:139–149.
91. Mikhailik A, Mazella J, Liang S, Tseng L. Notch ligand-dependent gene expression in human endometrial stromal cells. Biochem Biophys Res Commun 2009; 388:479–482.
92. Kageyama R, Ohtsuka T, Kobayashi T. The Hes gene family: repressors and oscillators that orchestrate embryogenesis. Development 2007; 134: 1243–1251.
93. Hayashi K, Erikson DW, Tilford SA, Bany BM, Maclean JA II, Rucker EB III, Johnson GA, Spencer TE. Wnt genes in the mouse uterus: potential regulation of implantation. Biol Reprod 2009; 80:989–1000.
94. Xie H, Tranguch S, Jia X, Zhang H, Das SK, Dey SK, Kuo CJ, Wang H. Inactivation of nuclear Wnt-beta-catenin signaling limits blastocyst competency for implantation. Development 2008; 135:717–727.
95. Hilton DJ, Nicola NA, Waring PM, Metcalf D. Clearance and fate of leukemia-inhibitory factor (LIF) after injection into mice. J Cell Physiol 1991; 148:430–439.
96. Lee JH, Kim TH, Oh SJ, Yoo JY, Akira S, Ku BJ, Lydon JP, Jeong JW. Signal transducer and activator of transcription-3 (Stat3) plays a critical role in implantation via progesterone receptor in uterus. FASEB J 2013; 27:2553–2563.
97. Ernst M, Inglese M, Waring P, Campbell IK, Bao S, Clay FJ, Alexander WS, Wicks IP, Tarlinton DM, Novak U, Heath JK, Dunn AR. Defective gp130-mediated signal transducer and activator of transcription (STAT) signaling results in degenerative joint disease, gastrointestinal ulceration, and failure of uterine implantation. J Exp Med 2001; 194:189–203.
98. Sun X, Bartos A, Whitsett JA, Dey SK. Uterine deletion of gp130 or stat3 shows implantation failure with increased estrogenic responses. Mol Endocrinol 2013; 27:1492–1501.
99. Mohamet L, Heath JK, Kimber SJ. Determining the LIF-sensitive period for implantation using a LIF-receptor antagonist. Reproduction 2009; 138:827–836.
100. Nakamura H, Kimura T, Koyama S, Ogita K, Tsutsui T, Shimoya K, Taniguchi T, Koyama M, Kaneda Y, Murata Y. Mouse model of human infertility: transient and local inhibition of endometrial STAT-3 activation results in implantation failure. FEBS Lett 2006; 580: 2717–2722.
101. White CA, Zhang JG, Salamonsen LA, Baca M, Fairlie WD, Metcalf D, Nicola NA, Robb L, Dimitriadis E. Blocking LIF action in the uterus by using a PEGylated antagonist prevents implantation: a nonhormonal contraceptive strategy. Proc Natl Acad Sci U S A 2007; 104: 19357–19362.
102. Ghosh D, Sengupta J. Target-oriented anti-implantation approaches for pregnancy interception: experiences in the rhesus monkey model. Contraception 2005; 71:294–301.
103. Nichols J, Chambers I, Taga T, Smith A. Physiological rationale for responsiveness of mouse embryonic stem cells to gp130 cytokines. Development 2001; 128:2333–2339.
104. Song H, Lim H, Das SK, Paria BC, Dey SK. Dysregulation of EGF family of growth factors and COX-2 in the uterus during the preattachment and attachment reactions of the blastocyst with the luminal epithelium correlates with implantation failure in LIF-deficient mice. Mol Endocrinol 2000; 14:1147–1161.
105. Zhang S, Lin H, Kong S, Wang S, Wang H, Wang H, Armant DR. Physiological and molecular determinants of embryo implantation. Mol Aspects Med 2013; 34:939–980.
106. Curtis Hewitt S Goulding EH , Eddy EM , Korach KS . Studies using the estrogen receptor alpha knockout uterus demonstrate that implantation but not decidualization-associated signaling is estrogen dependent. Biol Reprod 2002; 67:1268–1277.
107. Kondoh E, Okamoto T, Higuchi T, Tatsumi K, Baba T, Murphy SK, Takakura K, Konishi I, Fujii S. Stress affects uterine receptivity through an ovarian-independent pathway. Hum Reprod 2009; 24:945–953.
108. Pan H, Deng Y, Pollard JW. Progesterone blocks estrogen-induced DNA synthesis through the inhibition of replication licensing. Proc Natl Acad Sci U S A 2006; 103:14021–14026.
109. Jeong JW, Lee HS, Lee KY, White LD, Broaddus RR, Zhang YW, Vande Woude GF, Giudice LC, Young SL, Lessey BA, Tsai SY, Lydon JP, et al. Mig-6 modulates uterine steroid hormone responsiveness and

exhibits altered expression in endometrial disease. Proc Natl Acad Sci U S A 2009; 106:8677–8682.
110. Benson GV, Lim H, Paria BC, Satokata I, Dey SK, Maas RL. Mechanisms of reduced fertility in Hoxa-10 mutant mice: uterine homeosis and loss of maternal Hoxa-10 expression. Development 1996; 122:2687–2696.
111. Dunlap KA, Filant J, Hayashi K, Rucker EB III, Song G, Deng JM, Behringer RR, DeMayo FJ, Lydon J, Jeong JW, Spencer TE. Postnatal deletion of Wnt7a inhibits uterine gland morphogenesis and compromises adult fertility in mice. Biol Reprod 2011; 85:386–396.
112. Franco HL, Dai D, Lee KY, Rubel CA, Roop D, Boerboom D, Jeong JW, Lydon JP, Bagchi IC, Bagchi MK, DeMayo FJ. WNT4 is a key regulator of normal postnatal uterine development and progesterone signaling during embryo implantation and decidualization in the mouse. FASEB J 2012; 25:1176–1187.